LETTER

A three-dimensional human neural cell culture model of Alzheimer's disease

Se Hoon Choi[1]*, Young Hye Kim[1,2]*, Matthias Hebisch[1,3], Christopher Sliwinski[1], Seungkyu Lee[4], Carla D'Avanzo[1], Hechao Chen[1], Basavaraj Hooli[1], Caroline Asselin[1], Julien Muffat[5], Justin B. Klee[1], Can Zhang[1], Brian J. Wainger[4], Michael Peitz[3], Dora M. Kovacs[1], Clifford J. Woolf[4], Steven L. Wagner[6], Rudolph E. Tanzi[1] & Doo Yeon Kim[1]

Alzheimer's disease is the most common form of dementia, characterized by two pathological hallmarks: amyloid-β plaques and neurofibrillary tangles[1]. The amyloid hypothesis of Alzheimer's disease posits that the excessive accumulation of amyloid-β peptide leads to neurofibrillary tangles composed of aggregated hyperphosphorylated tau[2,3]. However, to date, no single disease model has serially linked these two pathological events using human neuronal cells. Mouse models with familial Alzheimer's disease (FAD) mutations exhibit amyloid-β-induced synaptic and memory deficits but they do not fully recapitulate other key pathological events of Alzheimer's disease, including distinct neurofibrillary tangle pathology[4,5]. Human neurons derived from Alzheimer's disease patients have shown elevated levels of toxic amyloid-β species and phosphorylated tau but did not demonstrate amyloid-β plaques or neurofibrillary tangles[6–11]. Here we report that FAD mutations in β-amyloid precursor protein and presenilin 1 are able to induce robust extracellular deposition of amyloid-β, including amyloid-β plaques, in a human neural stem-cell-derived three-dimensional (3D) culture system. More importantly, the 3D-differentiated neuronal cells expressing FAD mutations exhibited high levels of detergent-resistant, silver-positive aggregates of phosphorylated tau in the soma and neurites, as well as filamentous tau, as detected by immunoelectron microscopy. Inhibition of amyloid-β generation with β- or γ-secretase inhibitors not only decreased amyloid-β pathology, but also attenuated tauopathy. We also found that glycogen synthase kinase 3 (GSK3) regulated amyloid-β-mediated tau phosphorylation. We have successfully recapitulated amyloid-β and tau pathology in a single 3D human neural cell culture system. Our unique strategy for recapitulating Alzheimer's disease pathology in a 3D neural cell culture model should also serve to facilitate the development of more precise human neural cell models of other neurodegenerative disorders.

To develop human neural progenitor cells (hNPCs) that produce high levels of toxic amyloid-β species, we overexpressed human β-amyloid precursor protein (APP) or APP and presenilin 1 (PSEN1), containing FAD mutations. We first generated polycistronic lentiviral constructs designed to express human APP with both K670N/M671L (Swedish) and V717I (London) FAD mutations (APPSL) or APPSL and PSEN1 with ΔE9 FAD mutation (PSEN1(ΔE9)) (Fig. 1a). These FAD lentiviral constructs were transfected into ReNcell VM human neural stem (ReN) cells (Millipore). The transfected cells with GFP (ReN-G), mCherry (ReN-m), APPSL-GFP (ReN-GA), APPSL-GFP/PSEN1(ΔE9)-mCherry (ReN-mGAP), APPSL-PSEN1(ΔE9)-mCherry (ReN-mAP) or GFP/APPSL-PSEN1(ΔE9)-mCherry (HReN-mGAP) were enriched on the basis of GFP and/or mCherry signals using fluorescence-activated cell sorting (FACS) (Extended Data Fig. 1a–c, f). Western blot analysis revealed high expression of PSEN1(ΔE9), APP and APP carboxy-terminal fragments in ReN cells with FAD mutations (FAD ReN cells, Extended Data Fig. 1e).

As previously reported[12–14], most ReN cells differentiated into neuronal and glial cells within 3 weeks (Extended Data Figs 1d and 2a). Immunofluorescence staining confirmed punctate localization of VGluT1 (vesicular glutamate transporter 1), a presynaptic marker, along with dendritic processes (Extended Data Fig. 2b). Quantitative real-time PCR (qPCR) array analysis showed robust increases of neuronal and glial marker genes (Extended Data Fig. 2c). Reverse-transcription–PCR (RT–PCR) analysis also showed a dramatic increase of 4-repeat adult tau isoforms following differentiation (Extended Data Fig. 2d). The differentiated ReN cells
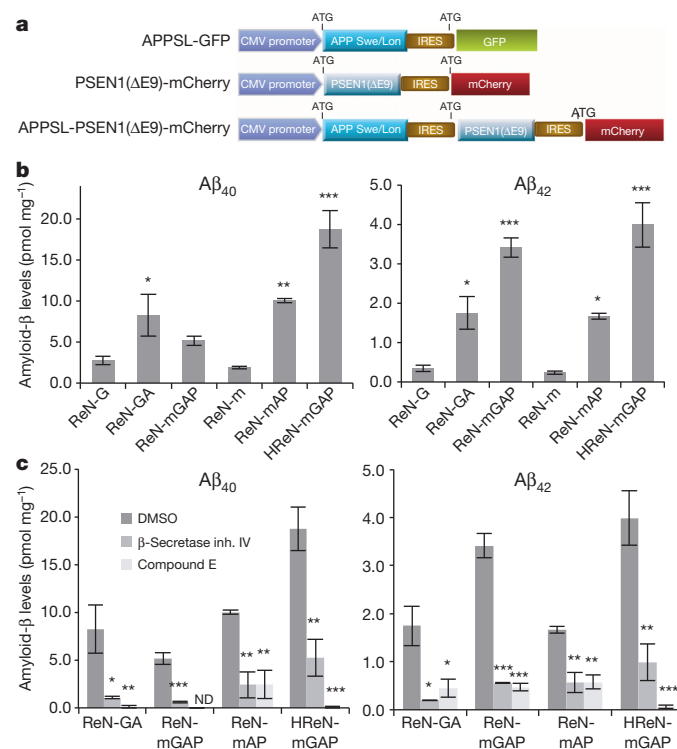
Figure 1 | Generation of hNPCs with multiple FAD mutations. a, Diagrams showing lentiviral internal ribosome entry sites (IRES) constructs. CMV, cytomegalovirus. **b**, Increased $A\beta_{40}$ and $A\beta_{42}$ levels in 6-week differentiated FAD ReN cells. Amyloid-β levels in conditioned media were normalized to total protein levels. *$P < 0.05$; **$P < 0.01$; ***$P < 0.001$; ANOVA followed by a post hoc Dunnett's test; $n = 3$ per each sample. **c**, Amyloid-β levels are dramatically decreased in FAD ReN cells after treatment with 1 μM β-secretase inhibitor IV or 3.7 nM compound E. Mean ± s.e.m.; *$P < 0.05$; **$P < 0.01$; ***$P < 0.001$; ANOVA followed by a post hoc Dunnett's test; $n = 3$ per each sample; ND, not detected.

[1]Genetics and Aging Research Unit, MassGeneral Institute for Neurodegenerative Disease, Massachusetts General Hospital, Harvard Medical School, Charlestown, Massachusetts 02129, USA. [2]Division of Mass Spectrometry Research, Korea Basic Science Institute, Cheongju-si, Chungbuk 363-883, South Korea. [3]Institute of Reconstructive Neurobiology, Life and Brain Center, University of Bonn and Hertie Foundation, 53127 Bonn, Germany. [4]FM Kirby Neurobiology Center, Boston Children's Hospital and Harvard Stem Cell Institute, Boston, Massachusetts 02115, USA. [5]The Whitehead Institute for Biomedical Research, Cambridge, Massachusetts 02142, USA. [6]Department of Neurosciences, University of California, San Diego, La Jolla, California 92093, USA.
*These authors contributed equally to this work.

exhibit voltage-gated potassium and sodium currents after 29 days of differentiation (Extended Data Fig. 2e–h), as previously reported[12,13].

We measured levels of the 40-amino-acid and 42-amino-acid amyloid-β isoforms ($A\beta_{40}$ and $A\beta_{42}$) in conditioned media after 6-week differentiation. FAD ReN cells revealed dramatic increases in $A\beta_{40}$ ($\sim$9-fold) and $A\beta_{42}$ ($\sim$17-fold) levels as compared to the control ReN cells (Fig. 1b and Extended Data Fig. 2i). The $A\beta_{42}$:$A\beta_{40}$ ratio was also increased ($\sim$5-fold) in ReN cells expressing PSEN1(ΔE9) (Fig. 1b). Treatment with β- or γ-secretase inhibitors markedly decreased amyloid-β levels (Fig. 1c) with no appreciable toxicity (data not shown). We confirmed that ReN

cells carry the APOE ε3/ε3 genotype, not the ε4 allele associated with Alzheimer's disease (Extended Data Fig. 2j).

In conventional 2D cultures, secreted amyloid-β diffuses into a large volume of media. We hypothesized that a 3D culture would accelerate amyloid-β deposition by limiting diffusion of amyloid-β, allowing for aggregation[15–17]. We chose BD Matrigel (BD Biosciences) as a 3D support matrix since it contains high levels of brain extracellular matrix proteins. For immunofluorescence and biochemical analyses, we set up thin- ($\sim$100–300 μm) and thick-layer ($\sim$4 mm) 3D culture models (Figs 2a and 3a). 3D-differentiated ReN cells displayed extensive processes after
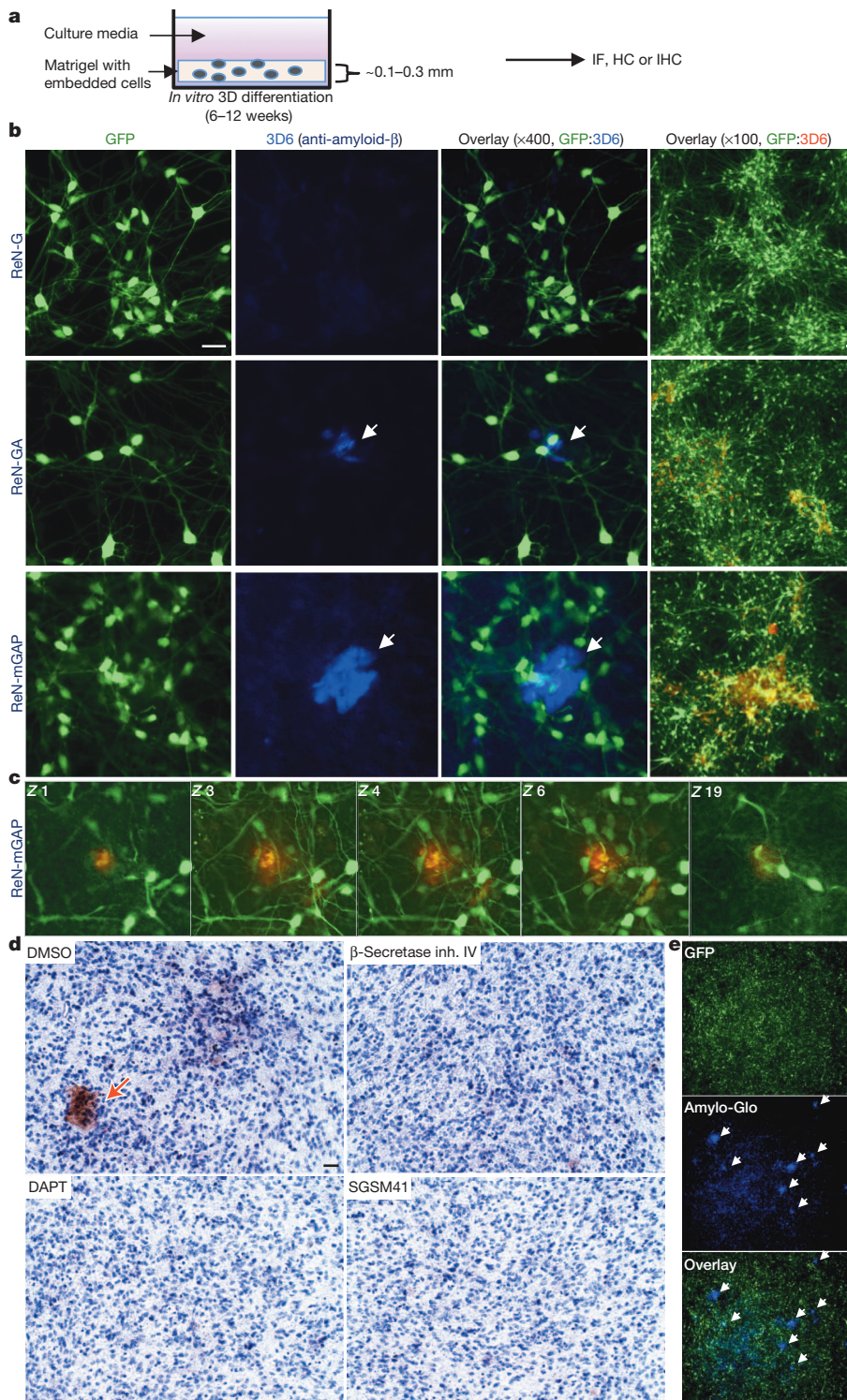
Figure 2 | Robust increases of extracellular amyloid-β deposits in 3D-differentiated hNPCs with FAD mutations. a, Thin-layer 3D culture protocol. HC, histochemistry; IF, immunofluorescence; IHC, immuno-histochemistry. **b**, Amyloid-β deposits in 6-week differentiated control and FAD ReN cells in 3D Matrigel (green, GFP; blue, 3D6; scale bar, 25 μm; arrowheads, extracellular amyloid-β deposits; right-most panels, 3D6 staining was pseudo-coloured to red). **c**, Select confocal Z-stack images of 3D6-positive amyloid-β deposits. Z-sections with an interval of 2 μm were captured and sections 1, 3, 4, 6 and 19 are shown (green, GFP; red, 3D6). **d**, IHC of amyloid-β deposits in ReN-mGAP cells. 3D-differentiated cells were treated with 1 μM β-secretase inhibitor IV, 500 nM DAPT, 500 nM SGSM41 or dimethyl sulphoxide (DMSO). Brown, 3,3′-diaminobenzidine (DAB, BA27); blue, haematoxylin; scale bar, 25 μm; arrowhead, large amyloid-β deposits. **e**, Detection of amyloid plaques in ReN-mGAP cells with Amylo-Glo (green, GFP; blue, Amylo-Glo; arrows, Amylo-Glo-positive aggregates).
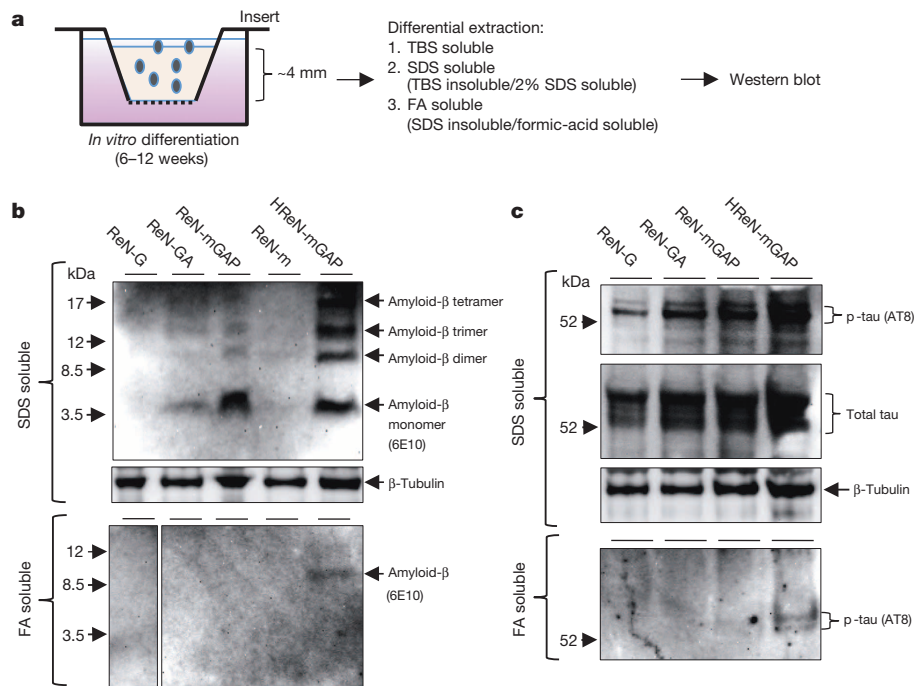
Figure 3 | Elevation of amyloid-β and p-tau levels in TBS-insoluble fractions of 3D-differentiated FAD hNPCs. a, A diagram showing a thick-layer 3D culture and detergent extraction protocols. **b**, Western blot of amyloid-β aggregates in 3D-differentiated ReN cells. 6E10-antibody-detected amyloid-β monomers, dimers, trimers and tetramers in SDS-soluble (upper panel) and formic-acid-soluble fractions (lower panel) from the control (ReN-G and -m) and the FAD ReN cells (ReN-GA, ReN-mGAP and HReN-mGAP) after 6 weeks of differentiation. **c**, Western blot of total and p-tau levels in SDS-soluble and formic-acid-soluble fractions.

2–6 weeks of differentiation (Supplementary Videos 1, 2 and 3). To demonstrate ReN-cell differentiation in thick-layer 3D cultures, paraffin-sectioned thick-layer 3D cultures were analysed by immunofluorescence with various neuronal markers (Extended Data Fig. 3). qPCR array data indicated that 3D cultures promote more neuronal and glial differentiation than 2D cultures (Extended Data Fig. 2c). We also observed a dramatic increase in the levels of 4-repeat adult tau isoforms in 3D cultures versus 2D (Extended Data Fig. 2d). These data demonstrate that 3D culture conditions not only promote neuronal maturation, but also increase adult tau isoform levels, which are essential for reconstituting tauopathy[18].

To detect amyloid-β deposits, 3D-differentiated ReN cells were stained with the anti-amyloid-β antibody 3D6 (Fig. 2b). Notably, confocal microscopy showed robust increases in extracellular amyloid-β deposits in FAD ReN cells (Fig. 2b). Confocal Z-sectioning exhibited 3D extracellular amyloid-β aggregates with diameters of 10–50 μm (Fig. 2c and Supplementary Video 4). Immunohistochemistry (IHC) with the BA27 anti-$A\beta_{40}$ antibody reconfirmed robust increases in amyloid-β aggregates and diffuse amyloid-β staining in FAD ReN cells (Fig. 2d and Extended Data Fig. 4a–c). Treatment with β- or γ-secretase inhibitors dramatically decreased amyloid-β deposits (Fig. 2d and Extended Data Fig. 4a). Accumulation of insoluble amyloid-β aggregates was also confirmed by Amylo-Glo, a fluorescent amyloid-specific dye (Biosensis; Fig. 2e and Extended Data Fig. 4d) and Congo red staining (data not shown). Treatment with the γ-secretase modulator SGSM41 (ref. 19) (Extended Data Table 1) markedly decreased the number of dense amyloid-β aggregates in 3D-differentiated FAD ReN cells, possibly by selectively decreasing the aggregation-prone $A\beta_{42}$ species (Fig. 2d and Extended Data Fig. 4a). For biochemical analysis, 3D-differentiated ReN cells were homogenized in Tris-buffered saline (TBS) and underwent a serial extraction protocol with 2% sodium dodecyl sulphate (SDS) and formic acid (Fig. 3a–c). Western blot analysis with the anti-amyloid-β antibody 6E10 revealed increased amyloid-β levels in SDS-soluble fractions of FAD ReN cells (Fig. 3b). In addition to a ~4-kDa amyloid-β monomer band, we observed amyloid-β dimer, trimer and tetramer bands in FAD ReN cells with high $A\beta_{42}$ levels (Fig. 3b). Amyloid-β dimers were detected in formic-acid-soluble fractions, especially in HReN-mGAP cells, which generated the highest levels of $A\beta_{40}$ and $A\beta_{42}$ (Fig. 3b).

In Alzheimer's disease, tau protein is hyperphosphorylated and abnormally accumulates in axons, dendrites and cell bodies[20]. To analyse

phosphorylated tau (p-tau) levels in FAD ReN cells, we performed western blot analysis with antibodies against p-tau (phosphorylated at Ser 199/Ser 202/Thr 205, AT8), and showed that p-tau levels were strongly increased in SDS-soluble fractions (Fig. 3c). Species of p-tau were also detected in formic-acid-soluble fractions in HReN-mGAP cells, which showed the highest accumulation of insoluble amyloid-β (Fig. 3b, c). Moderate increases of total tau levels were detected in FAD ReN cells, particularly in HReN-mGAP cells (Fig. 3c), which might be explained by robust increases in aggregated tau fractions. Notably, the γ-secretase inhibitor DAPT not only blocked amyloid-β generation but also inhibited p-tau levels in HReN-mGAP cells (Extended Data Fig. 5a, b). For further exploration of p-tau accumulation at the cellular level, we performed IHC staining with two different p-tau antibodies, AT8 and PHF1 (p-tau phosphorylated at Ser 396/Ser 404). We found dramatic increases in p-tau levels in a small portion of FAD ReN cells (Extended Data Fig. 5c–g). These cells displayed unusual morphologies, including beaded processes that are similar to the dystrophic neurites found in the brains of Alzheimer's disease patients (Extended Data Fig. 5c–e). Additionally, areas with highly dense p-tau-positive processes could only be detected in FAD ReN cells (Extended Data Fig. 5e, f). Treatment with either β- or γ-secretase inhibitors decreased p-tau-positive cell numbers in FAD ReN-mAP cells (Extended Data Fig. 5h). These data strongly suggest that p-tau accumulations in FAD ReN cells are induced by amyloid-β accumulation.

To enhance amyloid-β and p-tau pathologies, ReN-mAP cells with the top 1–2% mCherry signals were enriched by FACS (Extended Data Fig. 6a, b). Inhibitors of β- or γ-secretase decreased $A\beta_{40}$ and $A\beta_{42}$ levels in these cells while the γ-secretase modulator SGSM41 preferentially decreased toxic $A\beta_{42}$ levels and increased $A\beta_{38}$ levels (Extended Data Fig. 6c)[19]. PHF1 p-tau levels were also dramatically elevated in the enriched ReN-mAP cells (Fig. 4a, b). PHF1/MAP2 (anti-p-tau/anti-microtubule associated protein 2) and AT8/Tuj1(anti-p-tau/anti-β-tubulin type III) co-immunofluorescence analysis showed that p-tau levels were largely increased in neurites and neuronal cell bodies (Fig. 4a and Extended Data Fig. 7a). IHC analysis confirmed the dramatic increases in PHF1 p-tau levels in the enriched ReN-mAP cells (Fig. 4b). Notably, treatment with β- or γ-secretase inhibitors reduced the elevated p-tau levels, especially in neurite-like structures (Fig. 4b). Western blot analysis also showed that p-tau levels were robustly increased
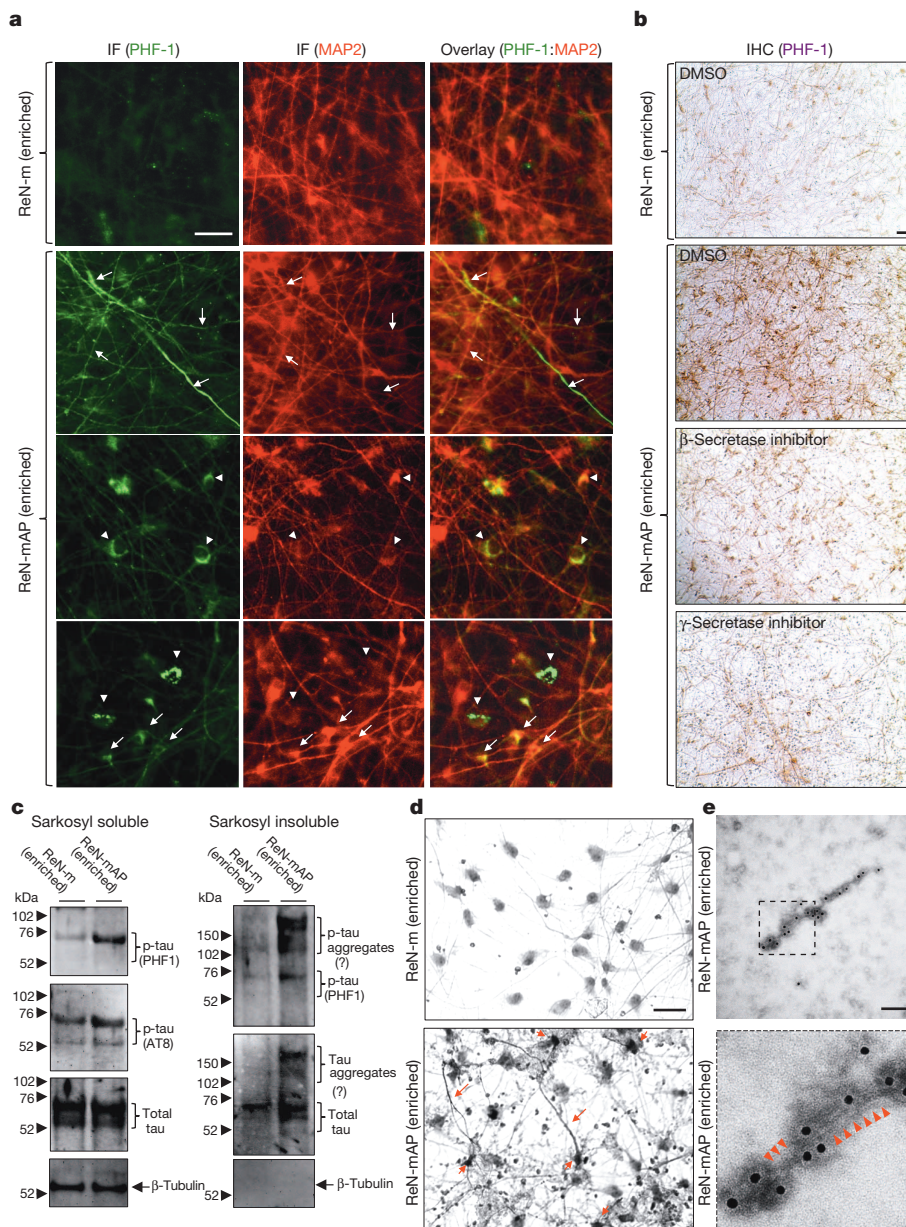
Figure 4 | Detection of aggregated p-tau in the enriched ReN-mAP cells. a, Immunofluorescence of p-tau and MAP2 in the enriched ReN-mAP and ReN-m cells after 3D differentiation. Green, p-tau (PHF1); red (pseudo-coloured), MAP2; scale bar, 25 μm; arrows, p-tau-positive neurites; arrowheads, p-tau-positive cell bodies. **b**, IHC of p-tau in the enriched ReN-mAP and ReN-m cells after 10-week 3D differentiation. The cells were treated with 1 μM β-secretase inhibitor IV, 3.7 nM compound E or DMSO during the final 2 weeks of the 3D differentiation. PHF1 antibody detected the elevated levels of p-tau in soma and neurites. Brown, p-tau; scale bar, 25 μm. **c**, Western blot of total and p-tau levels in 1% sarkosyl-soluble and -insoluble fractions. **d**, The modified Gallyas silver staining showed robust increases of strong silver deposits in cell bodies and neurite-like structures in the enriched ReN-mAP cells (lower panel) but not in the enriched ReN-m cells (upper panel). Scale bar, 25 μm; arrows indicate strong silver deposits in soma and neurites. **e**, Tau filaments were detected in sarkosyl-insoluble fractions from the enriched ReN-mAP cells by transmission electron microscopy after 7-week 3D differentiation. Black dots, anti-tau (tau46) antibodies labelled with immunogold anti-mouse antibodies; scale bar, 100 nm. Lower panel shows a digitally enlarged image (∼3.5 fold) (arrowheads indicate filamentous structures).

in the enriched ReN-mAP cells while total tau levels were unchanged (Extended Data Fig. 7b). A β-secretase inhibitor again decreased p-tau levels without affecting total tau levels (Extended Data Fig. 7b).

We further explored whether elevated p-tau proteins are aggregated in a manner similar to those observed in the degenerating neurons of Alzheimer's disease. Levels of p-tau were markedly increased in sarkosyl-insoluble fractions of the enriched ReN-mAP cells, but not in control ReN-m cells (Fig. 4c)[21]. The high-molecular-mass p-tau bands were detected only in sarkosyl-insoluble fractions of the enriched ReN-mAP cells, suggesting the presence of sarkosyl/SDS-resistant tau aggregates (Fig. 4c). Next, we performed modified Gallyas silver staining[22] on cells that had undergone 10 weeks of differentiation. Notably, strong silver depositions in cell bodies and neurite-like structures were detected in the enriched ReN-mAP, but not in the enriched ReN-m control cells (Fig. 4d, arrows). Finally, immunoelectron microscopy was employed to search for filamentous assemblies of tau protein in sarkosyl-insoluble fractions. Sarkosyl-insoluble fractions from 7-week differentiated ReN-mAP (enriched) and control ReN-G cells were analysed using transmission electron microscopy. Filamentous structures labelled with an anti-tau (tau46) antibody were detected in ReN-mAP cells, not in ReN-G cells (Fig. 4e and Extended Data Fig. 8a, b). The resulting p-tau

aggregates shared striking similarity with those observed in the brains of Alzheimer's disease patients[20]. We also found that the GSK3β inhibitors 1-azakenpaullone (1-AZA (ref. 23); Extended Data Fig. 9a, b) and SB415286 (SB41 (ref. 24), data not shown) dramatically decreased p-tau levels in the enriched ReN-mAP cells without changing total tau levels or significantly affecting amyloid-β levels (Extended Data Fig. 9c). These data indicate that GSK3β regulates amyloid-β-induced tauopathy downstream of amyloid-β deposition[25,26].

While increased p-tau levels have been reported in several Alzheimer's disease mouse models with FAD mutations, no somatic accumulated aggregates, detergent-resistant/silver-positive p-tau aggregates, nor immunogold-labelled detergent-resistant tau fibrils were observed[4,5]. The discrepancies between mouse FAD models and our 3D culture model might be a result of high levels of amyloid-β toxicity that can only be achieved in *in vitro* 3D culture conditions, or the differential tau gene structures in humans. We have shown that 3D-differentiated ReN cells exhibited a dramatic increase in mature human 4-repeat tau isoforms, which may be important for reconstituting tauopathy (Extended Data Fig. 2d). Indeed, a recent study showed that a rat FAD model, which has six tau isoforms similar to human, displayed some aspects of tauopathy[27]. Moreover, all aspects of tauopathy in our FAD hNPC models were

dramatically attenuated by β- or γ-secretase inhibitors, most probably through the inhibition of amyloid-β generation. These data support that tauopathy is driven by the excessive accumulation of amyloid-β engendered by FAD mutations in our model.

In summary, we have successfully recapitulated amyloid-β and tau pathologies in a 3D human neural cell culture system, which can be used as a platform for studying the pathogenic mechanisms of Alzheimer's disease and drug screening. Our 3D neural cell culture model also provides a unique platform to explore the molecular mechanisms by which p-tau pathologies are induced by toxic amyloid-β species in the absence of frontotemporal lobar degenerative tau mutations. Most importantly, we provide experimental validation of the amyloid hypothesis of Alzheimer's disease, which proposes that the accumulation of amyloid-β drives tauopathy. Our unique strategy for recapitulating Alzheimer's disease pathology in the 3D human neural cell culture model may also serve to facilitate the development of more precise human cellular models of other neurodegenerative disorders.

Online Content Methods, along with any additional Extended Data display items and Source Data, are available in the online version of the paper; references unique to these sections appear only in the online paper.

1. Tanzi, R. E. & Bertram, L. Twenty years of the Alzheimer's disease amyloid hypothesis: a genetic perspective. *Cell* **120,** 545–555 (2005).
2. Hardy, J. & Selkoe, D. J. The amyloid hypothesis of Alzheimer's disease: progress and problems on the road to therapeutics. *Science* **297,** 353–356 (2002).
3. Selkoe, D. Alzheimer's disease is a synaptic failure. *Science* **298,** 789–791 (2002).
4. Duff, K. Transgenic mouse models of Alzheimer's disease: phenotype and mechanisms of pathogenesis. *Biochem. Soc. Symp.* **67,** 195–202 (2001).
5. Chin, J. Selecting a mouse model of Alzheimer's disease. *Methods Mol. Biol.* **670,** 169–189 (2011).
6. Choi, S. H. & Tanzi, R. E. iPSCs to the rescue in Alzheimer's research. *Cell Stem Cell* **10,** 235–236 (2012).
7. Yagi, T. *et al.* Modeling familial Alzheimer's disease with induced pluripotent stem cells. *Hum. Mol. Genet.* **20,** 4530–4539 (2011).
8. Israel, M. A. *et al.* Probing sporadic and familial Alzheimer's disease using induced pluripotent stem cells. *Nature* **482,** 216–220 (2012).
9. Kondo, T. *et al.* Modeling Alzheimer's disease with iPSCs reveals stress phenotypes associated with intracellular Aβ and differential drug responsiveness. *Cell Stem Cell* **12,** 487–496 (2013).
10. Muratore, C. R. *et al.* The familial Alzheimer's disease APPV717I mutation alters APP processing and Tau expression in iPSC-derived neurons. *Hum. Mol. Genet.* **23,** 3523–3536 (2014).
11. Sproul, A. A. *et al.* Characterization and molecular profiling of PSEN1 familial Alzheimer's disease iPSC-derived neural progenitors. *PLoS ONE* **9,** e84547 (2014).
12. Donato, R. *et al.* Differential development of neuronal physiological responsiveness in two human neural stem cell lines. *BMC Neurosci.* **8,** 36 (2007).
13. Morgan, P. J. *et al.* Protection of neurons derived from human neural progenitor cells by veratridine. *Neuroreport* **20,** 1225–1229 (2009).
14. Mazemondet, O. *et al.* Quantitative and kinetic profile of Wnt/β-catenin signaling components during human neural progenitor cell differentiation. *Cell. Mol. Biol. Lett.* **16,** 515–538 (2011).
15. Li, H., Wijekoon, A. & Leipzig, N. D. 3D differentiation of neural stem cells in macroporous photopolymerizable hydrogel scaffolds. *PLoS ONE* **7,** e48824 (2012).
16. Lancaster, M. A. *et al.* Cerebral organoids model human brain development and microcephaly. *Nature* **501,** 373–379 (2013).
17. Tang-Schomer, M. D. *et al.* Bioengineered functional brain-like cortical tissue. *Proc. Natl Acad. Sci. USA* http://dx.doi.org/10.1073/pnas.1324214111 (August 11 2014).
18. Higuchi, M., Trojanowski, J. Q. & Lee, V. M.-Y. Tau protein and tauopathy. *Neuropsychopharmacology: The Fifth Generation of Progress* (eds Davis, K. L., Charney, D., Coyle, J. T. & Nemeroff, C.) 1339–1354 (Lippincott, Williams & Wilkins, 2002).
19. Wagner, S. L. *et al.* Soluble γ-secretase modulators selectively inhibit the production of the 42-amino acid amyloid β peptide variant and augment the production of multiple carboxy-truncated amyloid β species. *Biochemistry* **53,** 702–713 (2014).
20. Trojanowski, J. Q. & Lee, V. M.-Y. The role of tau in Alzheimer's disease. *Med. Clin. North Am.* **86,** 615–627 (2002).
21. Cras, P. *et al.* Neuronal and microglial involvement in β-amyloid protein deposition in Alzheimer's disease. *Am. J. Pathol.* **137,** 241–246 (1990).
22. Nadler, J. V. & Evenson, D. A. Use of excitatory amino acids to make axon-sparing lesions of hypothalamus. *Methods Enzymol.* **103,** 393–400 (1983).
23. Kunick, C., Lauenroth, K., Leost, M., Meijer, L. & Lemcke, T. 1-Azakenpaullone is a selective inhibitor of glycogen synthase kinase-3β. *Bioorg. Med. Chem. Lett.* **14,** 413–416 (2004).
24. Kirby, L. A. *et al.* Glycogen synthase kinase 3 (GSK3) inhibitor, SB-216763, promotes pluripotency in mouse embryonic stem cells. *PLoS ONE* **7,** e39329 (2012).
25. Phiel, C. J., Wilson, C. A., Lee, V. M.-Y. & Klein, P. S. GSK-3α regulates production of Alzheimer's disease amyloid-β peptides. *Nature* **423,** 435–439 (2003).
26. Jaworski, T. *et al.* GSK-3α/β kinases and amyloid production *in vivo. Nature* **423,** 435–439 (2003).
27. Cohen, R. M. *et al.* A transgenic Alzheimer rat with plaques, tau pathology, behavioral impairment, oligomeric Aβ, and frank neuronal loss. *J. Neurosci.* **33,** 6245–6256 (2013).

METHODS

Cell lines, media and reagents. ReNcell VM human neural precursor (ReN) cells were purchased from EMD Millipore (Billerica, MA, USA). The cells were plated onto BD Matrigel (BD Biosciences, San Jose, CA, USA)-coated T25 cell culture flasks (BD Biosciences, San Jose, CA, USA) and maintained in DMEM/F12 (Life Technologies, Grand Island, NY, USA) media supplemented with $2\,\mu g\,ml^{-1}$ heparin (StemCell Technologies, Vancouver, Canada), 2% (v/v) B27 neural supplement (Life Technologies, Grand Island, NY, USA), $20\,\mu g\,ml^{-1}$ EGF (Sigma-Aldrich, St Louis, MO, USA), $20\,\mu g\,ml^{-1}$ bFGF (Stemgent, Cambridge, MA, USA) and 1% (v/v) penicillin/streptomycin/amphotericin-b solution (Lonza, Hopkinton, MA, USA) in a CO_2 cell culture incubator. The cell culture media were changed every 3 days until the cells were confluent. For 2D neuronal/glial differentiation, the cells were plated onto either Matrigel-coated 24-well or 6-well plates with DMEM/F12 differentiation media supplemented with $2\,\mu g\,ml^{-1}$ heparin, 2% (v/v) B27 neural supplement, and 1% (v/v) penicillin/streptomycin/amphotericin-b solution without growth factors. One half volume of the differentiation media was changed every 3 days for 3–7 weeks. DAPT, compound E and β-secretase inhibitor IV were purchased from EMD Millipore; N-lauroylsarcosine (Sarkosyl) from Sigma-Aldrich; haematoxylin QS from Vector Laboratories (Burlingame, CA, USA); and Amylo-Glo from Biosensis (Thebarton, Australia). SGSM41 is an aminothiazole-bridged heterocycle-containing soluble γ-secretase modulator (SGSM) similar in structure to those published recently[19]. SGSM41 has the typical characteristics of this series of SGSM molecules that potently inhibit the production of $A\beta_{42}$ and to a lesser degree $A\beta_{40}$, while concomitantly increasing the generation of shorter amyloid-β peptide species such as $A\beta_{38}$ and $A\beta_{37}$. The structure and the detailed properties are included in Extended Data Table 1.

Complementary DNA constructs and viral packaging. The construct encoding full-length human β-amyloid precursor protein (APP_{695}) with the V717I (London) mutation was obtained from O. Berezovska (Massachusetts General Hospital, Boston, MA, USA; GenBank accession no. NM_201414). The human presenilin 1 (PSEN1) construct with ΔE9 mutation was a gift from J. Hardy (NIH, Bethesda, MD, USA; GenBank accession no. NM_000021). To introduce K670N/M671L (Swedish) mutations into the APP_{695} (London) gene, we performed a site-directed mutagenesis using a mutagenic primer set, 5′-CGGAGGAGATCTCTGAAGTGAATTTGGA TGCAGAATTCCGA-3′ and 5′-TCGGAATTCTGCATCCAAATTCACTTCAG AGATCTCCTCC G-3′ by using the QuikChange Site-Directed Mutagenesis Kit (Agilent Technologies, Santa Clara, CA, USA). APP (Swedish/London) and/or PSEN1(ΔE9) cDNAs were then PCR-amplified with Pfu (New England Biolabs, Ipswich, MA, USA) and cloned into lentiviral polycistronic CSCW-IRES-GFP or CSCW-IRES-mCherry vectors to generate CSCW-APP-GFP, CSCW-PSEN1(ΔE9)-mCherry and CSCW-APP-IRES-PSEN1(ΔE9)-IRES-mCherry. The parental CSCW-IGs vector was provided by Massachusetts General Hospital (MGH) viral core. The primers used for the cloning were: APP, 5′-CACCGCTAGCCAGGGTCGCGA ATGCTGC-3′ and 5′-GGCGTCGACCTAGTTCTGCATCTGCTC-3′; PSEN1, 5′-CACCGCTAGCAGTTGCTCCAATGACAGAGTTAC-3′ and 5′-GACCTCGAG CTAGATATAAAATTGATGGAATGC-3′. The amplified APP or PSEN1 genes were double-digested with NheI/SalI or NheI/XhoI and ligated to either CSCW-IRES-GFP or CSCW-IRES-mCherry vectors. To make CSCW-APP-IRES-PSEN1(ΔE9)-IRES-mCherry vector, the APP-IRES segment of CSCW-APP-IRES-GFP vector was PCR-amplified with 5′-CACCGCTAGCCAGGGTCGCGAATGCTGC-3′ and 5′-GGCGCTAGCGGTTGTGGCCATATTATCATC-3′ primers, digested with NheI and cloned into the NheI site of CSCW-PSEN1(ΔE9)-mCherry vector. All the newly constructed vectors were confirmed by sequencing (MGH sequence core, Charlestown, MA, USA). Viral packaging and titre determination were performed by MGH viral core (Charlestown, MA, USA).

Viral infection of ReN cell VM. To transfect the ReN cells with the lentiviral constructs, 50–100 μl viral solution ($1 \times 10^6\,TU\,ml^{-1}$) were added to 85% confluent proliferating ReN cells in 6-well dishes, incubated for 24 h, and washed three times to stop the infection. The expression of the infected genes was confirmed by mCherry or GFP expression by fluorescence microscopy and western blot analysis.

FACS enrichment of the transfected ReN cells. The infected ReN cells were washed with PBS and then incubated with Accutase (Millipore) for 5 min. The cell pellets were resuspended in PBS supplemented with 2% serum replacement solution (Life Technologies) and 2% B27, and then passed through a cell strainer filter (70 μm Nylon, BD Biosciences). The cell concentrations were adjusted to 2×10^6 cells per ml and then enriched by using FACSAria cell sorter (Broad Institute of MIT and Harvard, Cambridge, MA, USA). GFP and/or mCherry channels were used to detect the expression of the transfected genes in the individual cells. The sorted/enriched cells were maintained in normal proliferation media.

Amyloid-β ELISA. $A\beta_{40}$ and $A\beta_{42}$ levels were mainly measured by Human/Rat amyloid-β ELISA Kit from Wako (Osaka, Japan). The conditioned media from undifferentiated or differentiated ReN cells were collected and diluted by 1:10 or 1:100 with a dilution buffer provided by the manufacturer. A Synergy 2 ELISA plate reader (BioTek, Winooski, VT, USA) was used to quantify $A\beta_{40}$ and $A\beta_{42}$ ELISA signals. To simultaneously measure $A\beta_{38}$, $A\beta_{40}$ and $A\beta_{42}$ levels, a multi-array electrochemiluminescence ELISA kit was used (Meso Scale Discovery, Rockville, MD, USA).

APOE genotyping. Genomic DNA (5 ng) isolated from undifferentiated ReN-m and ReN-mAP cells was PCR amplified using TaqMan probes for the two APOE SNP markers (rs429358, catalogue no. C_3084793_20 and rs7412, catalogue no. C_904973_10) using TaqMan Universal Master Mix II (Life Technologies). DNA samples of known APOE ε4 genotypes (in duplicate) were used as controls to obtain the genotype clusters, and all the samples were PCR amplified on a CFX384 thermal cycler (Bio-Rad, Hercules CA, USA).

3D cell cultures and differentiation. For thin-layer 3D cultures, BD Matrigel stock solution (BD Biosciences) was diluted with ice-cold ReN cell differentiation medium (1:15 dilution ratio) and then vortexed with the cell pellets for 20 s. The final cell concentration for the mixture was approximately 2×10^6 cells per ml. The cell/Matrigel mixtures were immediately transferred into either Optilux Black/Clear bottom 96-well plates (100 μl in each well, BD Biosciences) or 8-chamber well Lab-Tek II coverglass plates (200 μl in each well, Thermo Scientific, Rockford, IL, USA) using pre-chilled pipettes. The plates were incubated for 1 h at 37 °C to form thin-layer (100–300 μm) 3D gels at the bottom of the plates and the media were changed. The 3D-plated cells were differentiated for 4–12 weeks depending on the experiments; media was changed every 3–4 days. For thick-layer 3D cultures, BD Matrigel solution was diluted with the same volume of the ice-cold ReN cell differentiation medium (1:2 dilution ratio) and vortexed with ReN cell pellets for 20 s. The final cell concentration for the mixture was approximately 1×10^7 cells per ml. Four-hundred microlitres of the cell/Matrigel mixtures were immediately transferred into tissue culture inserts (ThinCerts, 0.4 μm pore size, Greiner Bio-One, Monroe, NC, USA) and then placed in 24-well plates (BD Biosciences). After 1 h incubation at 37 °C, 1 ml of the pre-warmed differentiation media was added and the cultures were maintained for 4–12 weeks; media was changed every 3–4 days. For drug treatments, differentiation media containing either 1 μM β-secretase inhibitor IV, 1 μM DAPT, 3.7 nM compound E or the same volumes of DMSO were added to 4–6-week differentiated 3D-cultured ReN cells and then maintained for an additional 2–3 weeks. The cells were either fixed with 4% paraformaldehyde (PFA) or harvested for extraction and western blot analysis.

Paraffin embedding and sectioning of thick-layer 3D cultures. For paraffin embedding, 3D thick layer cultures were fixed with 4% PFA at room temperature overnight. The PFA-fixed Matrigel was then transferred to a plastic Tissue-Tek Cryomold (Sakura Finetek, Torrance, CA, USA), preloaded with 60 °C liquefied HistoGel (Thermo Scientific). After positioning the fixed 3D Matrigel at the centre, the whole Cryomold with Histogel/Matrigel was transferred on ice and then incubated for 15 min until the Histogel was solidified. The Histogel/Matrigel complex was then further fixed with 4% PFA at 4 °C overnight, washed five times with PBS, and sent for paraffin embedding (MGH pathology core, Charlestown, MA, USA). The paraffin blocks were then cut into 10 μm sections (Leica SM2010R sliding microtome, Leica Microsystems Inc., Buffalo Grove, IL, USA), mounted on polylysine-coated glass slides (Thermo Scientific), and incubated at 45 °C overnight. The sections were deparaffinized by two changes of xylene for 5 min each and then serially transferred to 100%, 90%, 70% ethanol solution for 1 min each. The sections were then rinsed with distilled water for 5 min. For immunofluorescence and IHC, the antigen retrieval was performed by heating the slides for 30 min in Citrate-EDTA Buffer containing 10 mM citric acid (pH 6.2), 2 mM EDTA and 0.05% Tween-20.

Immunofluorescence staining. For immunofluorescence of 3D-cultured ReN cells, thin-layer 3D cultures were fixed with 4% PFA at room temperature for 24 h. The fixed cells were then permeabilized and blocked by incubating with a blocking solution containing 50 mM Tris (pH 7.4), 0.1% Tween-20, 4% donkey serum, 1% BSA, 0.1% gelatin and 0.3 M glycine at 4 °C for 12 h. After washing with TBS buffer containing 0.1% (v/v) Tween-20 (TBST), the 3D cultures were incubated with primary antibodies in the blocking solution at 4 °C for 24 h. After washing three times with TBST, the cells were then incubated with TBST overnight with gentle rocking at 4 °C and then further incubated with AlexaFluor secondary antibodies (Life Technologies) overnight at 4 °C. To avoid fluorescence quenching, a drop of anti-fade gold (Life Technologies) was added on top of the fixed/stained thin-layer 3D cultures before imaging. The fluorescence images were captured by an Olympus DSU confocal microscope (Olympus USA, Center Valley, PA, USA) and the image analysis and 3D reconstitution were performed with ImageJ (a public domain image analysis software), IPlabs (BioVision Technologies, Exton, PA, USA) and MetaMorph (Molecular Devices, Sunnyvale, CA, USA) software. The following antibody dilution rates were used in this study: 3D6 anti-amyloid-β antibody (1:500, a gift from Lilly); anti-β-tubulin type III (Tuj1, 1:200, Abcam, Cambridge, MA, USA); anti-GFAP antibody (1:2,000, DAKO, Carpinteria, CA, USA; 1:200, Antibodies Incorporated, Davis, CA, USA); AT8 anti-p-tau antibody (1:40, Thermo Scientific); PHF1 anti-phospho tau antibody (1:1,000, courtesy of P. Davies); anti-tau$_{46}$ antibody (1:200, Cell Signaling Technology); anti-GluR2 (1:100, Antibodies Incorporated); anti-MAP2

antibodies (1:400, Millipore; 1:200, Cell Signaling Technology); anti-tyrosine hydroxylase (1:100, Cell Signaling Technology); anti-NR2B (1:100, Antibodies Incorporated); anti-GABA(B)R2 (1:100, Cell Signaling Technology); AlexaFluor 350/488/568 anti-mouse, -rabbit and -chicken secondary antibodies (1:200, Life Technologies).

Immunohistochemical staining. For IHC, thin-layer 3D cultures were permeabilized and blocked by incubating with the blocking solution at 4 °C for 12 h. To block endogenous peroxidase activities, the cultures were incubated with 0.05% (v/v) H_2O_2 solution in TBS for 5 min at room temperature, washed with TBST three times and incubated with the blocking solution for 2 h at room temperature. After incubating with the primary antibody solutions for 24 h at 4 °C, the cultures were washed five times with TBST and then incubated with ImmPRESS anti-mouse or -rabbit Ig (ImmPRESS Peroxidase Polymer Detection Kit, Vector Laboratories, Burlingame, CA, USA) for 30–60 min. The cultures were washed five times for 10 min each with TBST and developed by using ImmPACT DAB Peroxidase Substrate kit (Vector Laboratories). The following antibodies and dilution rates have been used in this study: BA27 anti-Aβ_{40} antibody horseradish peroxidase (HRP)-conjugate (1:2, Wako Chemicals USA, Richmond, VA, USA); BC05 anti-Aβ_{42} antibody HRP-conjugate (1:2, Wako Chemicals USA); AT8 anti-p-tau antibody (1:40, Thermo Scientific); PHF1 anti-p-tau antibody (1:1,000), anti-MAP2 antibody (1:200, Cell Signaling Technology); ImmPRESS anti-mouse and -rabbit Ig HRP polymer conjugates (1:2, Vector Laboratories).

Differential detergent extraction for western blot. The thick-layer 3D cultures of ReN cells were homogenized with TBS extraction buffer containing 50 mM Tris (pH 7.4), 150 mM NaCl, 1 mM NaVO$_3$, 1 mM NaF, a protease inhibitor mixture (Roche Molecular Biochemicals), a phosphatase inhibitor cocktail (Thermo Scientific), 2 mM PNT (EMD Millipore) and 1 mM phenylmethylsulphonyl fluoride (PMSF, Sigma-Aldrich) by using a battery-operated spinning homogenizer (MIDSCI, St Louis, MO, USA). After incubation on ice for 10 min, the samples were centrifuged for 1 h at 100,000g to get TBS-soluble fractions. The TBS-insoluble pellets were then resuspended in 2% SDS extraction buffer containing 50 mM Tris (pH 7.4), 150 mM NaCl, 2% SDS, 1% Triton X-100, 1 mM NaVO$_3$, 1 mM NaF, a protease inhibitor mixture (Roche Molecular Biochemicals), a phosphatase inhibitor cocktail (Thermo Scientific), 2 mM PNT (EMD Millipore) and 1 mM PMSF (Sigma-Aldrich) and incubated on ice for an additional 30 min. The samples were centrifuged for 1 h at 100,000g and the supernatant fractions were collected as TBS-insoluble/2% SDS-soluble fractions. The 2% SDS-insoluble pellets were briefly washed with SDS extraction buffer and then further extracted with 90% formic acid (Sigma-Aldrich) on ice and centrifuged for 1 h at 100,000g to produce TBS-insoluble/2% SDS-insoluble/formic-acid-soluble fractions. The formic acid fractions were enriched by using SpeedVac and neutralized by 2 M Tris-Cl buffer (pH 8.3). Protein levels of SDS-soluble fractions were used to normalize the total protein levels in TBS and formic acid fractions. Purification of sarkosyl-insoluble tau was performed as previously described[28,29] with modifications. TBS-insoluble pellets were resuspended in 1% sarkosyl/RIPA buffer containing 50 mM Tris (pH 7.4), 150 mM NaCl, 0.5% w/v sodium deoxycholate, 2% v/v NP-40, 1% w/v N-lauroylsarcosine, a protease inhibitor mixture (Roche Molecular Biochemicals), a phosphatase inhibitor cocktail (Thermo Scientific), 1 mM NaF, 1 mM NaVO$_3$, 2 mM PNT (EMD Millipore) and 1 mM PMSF (Sigma-Aldrich) and incubated on ice for 1 h. The samples were then centrifuged for 1 h at 100,000g and the supernatant fractions were collected as 1% sarkosyl/RIPA-soluble fractions. The insoluble pellets were briefly washed two times with 1% sarkosyl/RIPA buffer, further extracted with 90% formic acid (Sigma-Aldrich) on ice and centrifuged for 1 h at 100,000g to produce 1% sarkosyl/RIPA-insoluble /formic-acid-soluble fractions.

Western blot analysis. 15–75 μg of protein were resolved on 12% Bis-Tris or 4–12% gradient Bis/Tris gels (Life Technologies) and the proteins were transferred to nylon membranes (Bio-Rad). For amyloid-β western blot analysis, the membranes were crosslinked with 0.5% glutaraldehyde solution before blocking. Western blot images were visualized by enhanced chemiluminescence (ECL). The images were captured by using BioMax film (Kodak, Rochester, NY, USA) or a VersaDoc imaging system (Bio-Rad) and quantitated by using QuantityOne software (Bio-Rad). Primary antibodies were used at the following dilutions: 6E10 anti-amyloid-β (1:300, Convance); anti-PSEN1 (1:1,000, Cell Signaling Technology); anti-α-tubulin (1:1,000, Cell Signaling Technology); anti-CNPase (1:1,000, Cell Signaling Technology); anti-β-secretase 1 (1:1,000, Cell Signaling Technology); C66 APP C-terminal antibody (1:2,000); AT8 anti-p-tau (1:100, Millipore); PHF1 anti-p-tau (1:500); anti-total tau (1:2,000, DAKO); anti-MAP2 (1:500, Millipore; 1:200, Cell Signaling); anti-NCAM (1:1,000, Cell Signaling); anti-synapsin I (1:500, Cell Signaling); anti-HSP70 (1:1,000, Enzo Life Sciences, Farmingdale, NY, USA) and anti-human mitochondrial antigen (1:500, Millipore).

Modified Gallyas silver staining. Gallyas silver staining was performed with a modified protocol described by Nadler et al.[22]. The PFA-fixed thin-layer 3D cultures were washed three times with deionized distilled water (DDW) for 5 min and

then incubated two times with a pretreating solution containing 4.5% (w/v) NaOH and 0.6% (w/v) ammonium nitrate. The cultures were then incubated with an impregnation solution containing 5.4% (w/v) NaOH, 6.4% (w/v) ammonium nitrate and 0.3% (w/v) silver nitrate for 10 min followed by three washes with a washing solution containing 1 ml of 0.0012% (w/v) ammonium nitrate, 0.5% (w/v) sodium carbonate and 28.5% (v/v) ethanol at 5-min intervals. The deposition of silver particles was detected by incubating with a developer solution with 0.012% (w/v) ammonium nitrate, 0.05% (w/v) citric acid, 0.56% (w/v) formalin and 9.5% (v/v) ethanol for 1–5 min. The reaction was stopped by adding 0.5% acetic acid.

Amylo-Glo staining. The fixed 3D thin-layer cultures of ReN cells were washed three times with saline and incubated with 0.001% (v/v) Amylo-Glo solution for 5 min in a dark environment. The cells were then washed with saline followed by three washings with DDW. To avoid fluorescence quenching, a drop of anti-fade gold (Life Technologies) was added on top of the stained cells. The Amylo-Glo fluorescence was measured with an Olympus DSU confocal microscope with Metamorph image analysis software (Olympus).

Congo red staining. Bennhold's Congo red staining protocol was used for staining paraffin sectioned 3D cultures with slight modification. The hydrated paraffin-sectioned 3D cultures were incubated with 1% Congo red solution (Sigma-Aldrich) for 60 min at room temperature. After briefly rinsing with distilled water three times, the sections were dipped several times into an alkaline alcohol solution (30% EtOH, 0.01% (w/v) NaOH) until the background was cleared. The slides were then washed twice with DDW.

RNA extraction, cDNA synthesis and quantitative RT–PCR (qPCR) analysis. Total RNAs were prepared by using RNeasy mini-columns (Qiagen, Valencia, CA, USA) according to the manufacturer's protocols. Complementary DNAs were synthesized by SuperScript III first-strand synthesis kit (Life Technologies). The pre-validated primer sets for neural markers were purchased from Real Time Primers, LLC (Elkins Park, PA, USA). The amplification was done in a final volume of 20 μl under the following conditions: 15 min at 95 °C and then 55 cycles at 95 °C for 10 s, 58 °C for 45 s and 72 °C for 45 s. The sizes of the qPCR products were confirmed by agarose gel electrophoresis. Biorad iCycler was used to determine count values for each sample. Gene expression levels were normalized against β-actin levels in each sample and the fold changes were calculated by setting the expression levels of each gene in undifferentiated control ReN-G cells as 1. The following are the neuronal and glial marker gene names and PCR product sizes: NCAM1 (neural cell adhesion molecule 1, 174 base pairs (bp)); SYT5 (synaptotagmin V, 171 bp); SLC17A7 (also known as VGLUT1, solute carrier family 17 (sodium-dependent inorganic phosphate co-transporter) member 7, 162 bp); GRIN2A (glutamate receptor, ionotropic, N-methyl D-aspartate 2A, 170 bp); EAAT3 (solute carrier family 1, member 1 (neuronal glutamate transporter), 165 bp); ACHE (acetylcholinesterase, 232 bp); SLC6A4 (solute carrier family 6 member 4 (neurotransmitter transporter, dopamine), 213 bp); GABRA1 (γ-aminobutyric acid (GABA) A receptor alpha 1, 165 bp); MAPT (microtubule-associated protein tau, 206 bp); S100β (S100 calcium binding protein, 157 bp); GFAP (glial fibrillary acidic protein, 183 bp); EAAT2 (solute carrier family 1, member 2 (EAAT2, glial), 158 bp); MBP (myelin basic protein, 183 bp); and ACTB (β-actin, 233 bp).

RT–PCR analysis of 3-repeat and 4-repeat tau levels. Relative levels of 3-repeat and 4-repeat tau mRNAs were determined by RT–PCR using the primer sets: forward 5′-AAGTCGCCGTCTTCCGCCAAG-3′; reverse 5′-GTCCAGGGACCCA ATCTTCGA-3′ as previously described[30]. The PCR amplification was performed in a final volume of 20 μl under the following conditions: 95 °C for 15 min, and then 30 cycles at 94 °C for 30 s, 60 °C for 30 s and 74 °C for 90 s with a final 10 min extension at 74 °C. RT–PCR products were analysed on 2% agarose gel: 4-repeat tau, 381 bp; 3-repeat tau, 288 bp.

Preparation of sarkosyl-insoluble tau fibrils for immunoelectron microscopy. Sarkosyl-insoluble tau fibrils were prepared from FAD-ReN (ReN-mAP (enriched)) cells, which were differentiated in 3D for 7 weeks[28,29]. 3D-cultured cell pellets were homogenized in one volume of TBS extraction buffer containing 50 mM Tris (pH 7.4), 150 mM NaCl, 1 mM NaVO$_3$, 1 mM NaF, a protease inhibitor mixture (Roche Molecular Biochemicals), a phosphatase inhibitor cocktail (Thermo Scientific), 2 mM PNT (EMD Millipore) and 1 mM PMSF (Sigma-Aldrich) by using a battery-operated spinning homogenizer (MIDSCI). TBS homogenates were then mixed and homogenized with one volume of 2× RIPA buffer containing 50 mM Tris (pH 7.4), 150 mM NaCl, 0.5% w/v sodium deoxycholate, 2% v/v NP-40, a protease inhibitor mixture (Roche Molecular Biochemicals), a phosphatase inhibitor cocktail (Thermo Scientific), 1 mM NaF, 1 mM NaVO$_3$, 2 mM PNT (EMD Millipore) and 1 mM PMSF (Sigma-Aldrich), and incubated on ice for 15 min. After centrifugation (18,000g for 20 min at 4 °C), 20% w/v N-lauroylsarcosine (sarkosyl) stock solution was added to the RIPA-soluble supernatant fraction to adjust the final sarkosyl concentration to 1%. After incubating at room temperature with gentle rocking for 1 h, RIPA/sarkosyl homogenates were then centrifuged for 1 h at 150,000g. The pellets were then resuspended in 10 μl of PBS (RIPA-soluble/sarkosyl-insoluble fraction). The

RIPA-insoluble pellets were further homogenized in H buffer containing 10 mM Tris (pH 7.4), 1 mM EGTA, 0.8 M NaCl, 10% w/v sucrose, a protease inhibitor mixture (Roche Molecular Biochemicals), a phosphatase inhibitor cocktail (Thermo Scientific), 1 mM NaF, 1 mM NaVO$_3$, 2 mM PNT (EMD Millipore) and 1 mM PMSF (Sigma-Aldrich) and then centrifuged at 18,000g for 20 min. 20% w/v N-lauroylsarcosine (sarkosyl) stock solution was added to adjust the final sarkosyl solution concentration to 1%. After incubating at room temperature with gentle rocking for 1 h, H buffer/sarkosyl homogenates were then centrifuged for 1 h at 150,000g and the pellets were resuspended in 10 μl of PBS (RIPA-insoluble/sarkosyl-insoluble fraction). Both RIPA-soluble/sarkosyl-insoluble and RIPA-insoluble/sarkosyl-insoluble fractions were used for immunoelectron microscopy. The same protocol was used to enrich sarkosyl-insoluble p-tau aggregates in Alzheimer's disease brain samples.

Immunogold staining of sarkosyl-insoluble tau. Immunoelectron microscopy was performed in the Microscopy Core of the Center for Systems Biology/Program in Membrane Biology (MGH, Boston, USA). The sarkosyl-insoluble fractions were resuspended in PBS, placed on formvar-carbon coated Ni grids and allowed to adsorb for 10 min. They were placed on drops of tau$_{46}$ antibody solution (1:25, Cell Signaling Technology) for 1 h at room temperature, then rinsed on drops of PBS and placed on drops of goat-anti-mouse 10 nm gold (Ted Pella, Redding, CA, USA) for 1 h. They were rinsed on drops of distilled water and stained for 1 min on drops of 2% phosphotungstic acid (Electron Microscopy Sciences, Hatfield, PA, USA). Grids were examined in a JEOL JEM 1011 transmission electron microscope at 80 kV.

Images were collected using an AMT digital imaging system (Advanced Microscopy Techniques, Danvers, MA, USA).

Electrophysiology. Whole-cell recordings were performed on differentiated ReN cells with an Axopatch 200A amplifier (Molecular Devices) and fire polished patch pipettes with resistances of 2–3 MΩ. Pipette solution was 140 mM KCl, 2 mM MgCl$_2$, 1 mM EGTA, 10 mM HEPES, 4 mM MgATP, 0.3 mM NaGTP, and 0.1 mM Na$_2$PhosCr, pH 7.2, adjusted with KOH. The external solution was 140 mM NaCl, 5 mM KCl, 2 mM CaCl$_2$, 2 mM MgCl$_2$, 10 mM HEPES, and 10 mM D-glucose, pH 7.4, adjusted with NaOH. Command protocols were generated and data were digitized with a Digidata 1440A A/D interface with pCLAMP10 software (Molecular Devices). Voltage errors were minimized by series resistance compensation (80%). During the recording, 500 nM tetrodotoxin was applied to isolate Na$^+$ currents by subtracting currents after and before tetrodotoxin application. The data were analysed by Clampfit (Molecular Devices) and Sigmaplot.

Statistics. All statistical analyses were performed using a two-tailed Student's t-test or one-way ANOVA followed by a post hoc Dunnett's test. Data in graphs are expressed as mean values ± s.e.m. Error bars represent s.e.m.

28. Planel, E. *et al.* Acceleration and persistence of neurofibrillary pathology in a mouse model of tauopathy following anesthesia. *FASEB J.* **23,** 2595–2604 (2009).
29. Julien, C., Bretteville, A. & Planel, E. Biochemical isolation of insoluble tau in transgenic mouse models of tauopathies. *Methods Mol. Biol.* **849,** 473–491 (2012).
30. Iovino, M., Patani, R., Watts, C., Chandran, S. & Spillantini, M. G. Human stem cell-derived neurons: a system to study human tau function and dysfunction. *PLoS ONE* **5,** e13947 (2010).
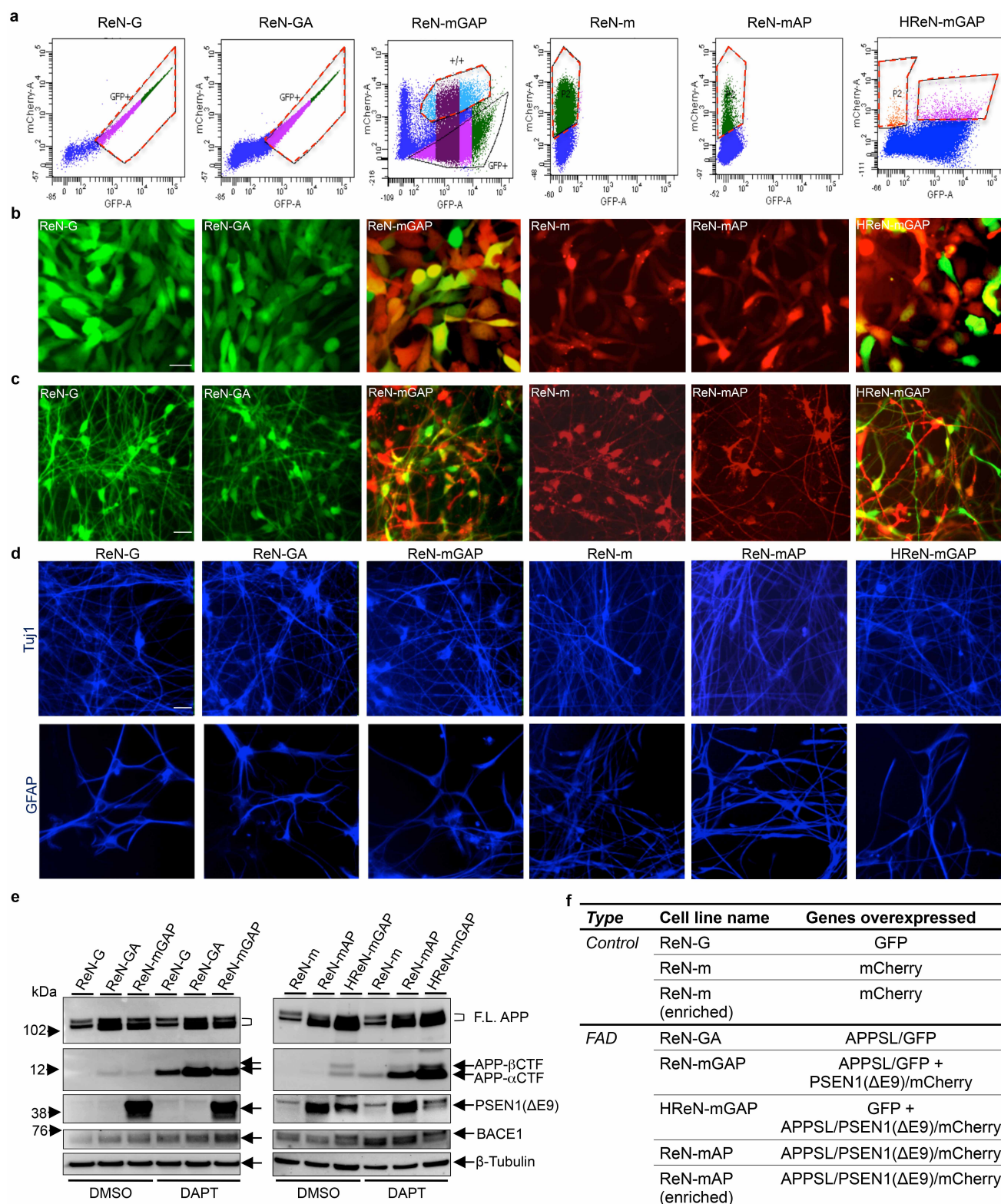
Extended Data Figure 1 | Generation of FACS-sorted ReN cells with FAD mutations. a, FACS sorting of ReNcell VM human neural stem (ReN) cells that were stably transfected with polycistronic GFP and/or mCherry lentiviral vector(s). The cells were then enriched based on GFP and/or mCherry signals by FACS (red-dotted boxes, the selected ranges of cells for the experiments; mCherry-A, area intensity of mCherry signal; GFP-A, area intensity of GFP signal). **b**, ReN cells stably expressing GFP alone (ReN-G), APPSL-GFP (ReN-GA), APPSL-GFP-PSEN1(ΔE9)-mCherry (ReN-mGAP), mCherry alone (ReN-m), APPSL-PSEN1(ΔE9)-mCherry (ReN-mAP) or GFP-APPSL-PSEN1(ΔE9)-mCherry (HReN-mGAP). Green, GFP; red, mCherry; scale bar, 25 μm. **c**, The representative fluorescence microscope images of ReN cells that were differentiated by growth-factor deprivation for 3 weeks (green, GFP; red, mCherry; scale bar, 25 μm). **d**, Immunofluorescence of neuronal (Tuj1) and glial markers (GFAP) in 3-week differentiated control and FAD ReN cells. Scale bar, 25 μm. **e**, Western blot of APPSL and PSEN1(ΔE9) expression in control (ReN-G and ReN-m) and FAD ReN (ReN-GA, ReN-mGAP and HReN-mGAP) cells. APP C-terminal fragment (CTF) levels were greatly increased by 500 nM DAPT treatments for 24 h. BACE1, β-secretase 1, F.L. APP, full-length APP. **f**, A table summarizing the control and FAD ReN cells generated for this study.

a

Undifferentiated lanes: ReN-G, ReN-GA, ReN-mGAP, ReN-m, ReN-mAP, HReN-mGAP

3-week differentiated lanes: ReN-G, ReN-GA, ReN-mGAP, ReN-m, ReN-mAP, HReN-mGAP

Blots (kDa): MAP2 (76), Tuj1 (102), NCAM (150, 102), Synapsin I (52, 52), GFAP (52), HSP70 (76)

Undifferentiated | 3-week differentiated

b

VGluT1 | MAP2 | Overlay | Enlarged

c

Type	Gene name	ReN-G, 2D-differentiated (fold increases)	ReN-G, 3D-differentiated (fold increases)
Neuronal	NCAM1	15.2 ± 3.1	39.7 ± 25.7
	SYT5	7.2 ± 0.7	3.6 ± 1.2
	SLC17A7 (VGLuT1)	3.8 ± 0.8	184.3 ± 64.5
	GRIN2A (NR2A)	2.6 ± 1.2	134.1 ± 63.4
	EAAT3	2.1 ± 0.5	45.1 ± 9.4
	ACHE	4.8 ± 1.9	4.6 ± 1.3
	SLC6A4	9.5 ± 3.8	87 ± 37.9
	GABRA1	4.9 ± 0.7	239.3 ± 57.9
	MAPT	33 ± 4.8	525.3 ± 156.9
Glial	S100β	7.6 ± 0.9	138.8 ± 42.2
	GFAP	17.3 ± 5.0	118 ± 34.9
	EAAT2	3.3 ± 0.2	107.1 ± 18.9
	MBP	4.2 ± 1.0	11.9 ± 5.9

d

Lanes: ReN-G, ReN-G, ReN-GA, ReN-mGAP, HReN-mGAP, ReN-m, ReN-mAP, ReN-G (3D-differentiated), Adult human brain

bp markers: 400, 300, 200

4R tau, 3R tau

Undiff. | 2D | 3D | Human brain

7-week differentiated

e

60 mV, −90 mV, −100 mV

f

+TTX

0.5 nA, 50 msec

g

0.2 nA, 2.5 msec

h

1 nA, 50 msec

i

Lanes: ReN-m, HReN-mGAP, ReN-m, ReN-mAP

kDa markers: 24, 17, 12, 8.5, 3.5

Aβ

j

Cell line	APOE genotype
ReN-m	ε3/ε3
ReN-mAP	ε3/ε3

Extended Data Figure 2 | Characterization of the control and FAD ReN cells. a, Western blot of neuronal (MAP2, Tuj1, NCAM, synapsin 1) and glial (GFAP) markers in undifferentiated and 3-week differentiated control and FAD ReN cells. **b**, Confocal immunofluorescence of presynaptic (VGluT1, green) and dendritic (MAP2, red (pseudo-coloured)) markers in 6-week differentiated control ReN-m cells. Top-left, top-right and bottom-left panels, ×100 magnification; bottom-right panel represents a digitally magnified image of the respective outlined region for better visualization of punctate structures. **c**, qPCR array analysis of neuronal and glial markers of 7-week differentiated control ReN-G cells. Gene expression levels were normalized against β-actin levels in each sample and the fold changes were calculated by setting the expression levels of each gene in undifferentiated control ReN-G cells as 1 ($n = 3$ for ReN-G whereas $n = 5$ for ReN-G in 3D differentiation). FAD ReN cells (HReN-mGAP and ReN-mAP) showed a similar pattern of increases in neuronal and glial markers (data not shown). **d**, Analysis of 4-repeat (4R) or 3-repeat (3R) tau isoforms in 7-week differentiated control ReN cells (ReN-G 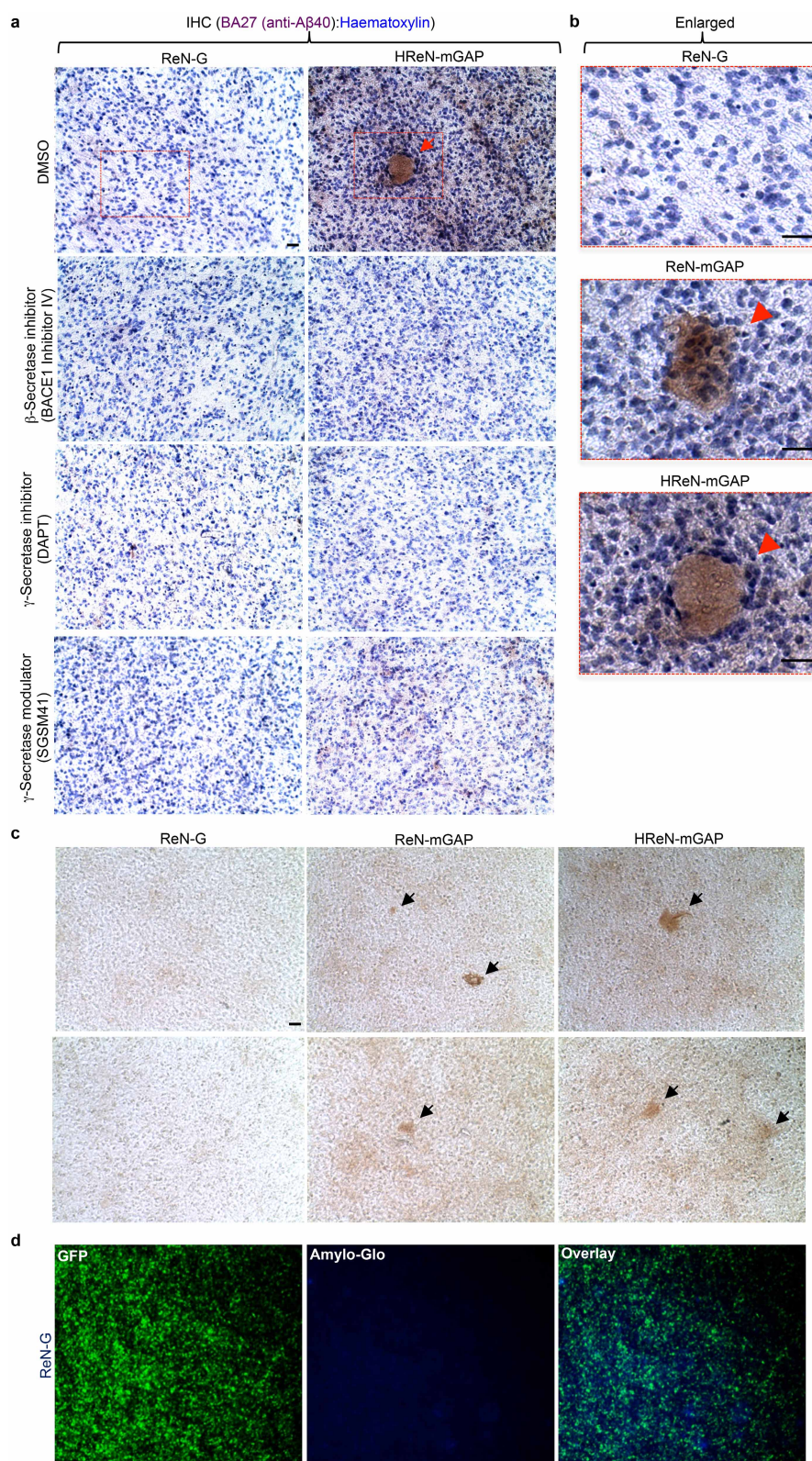and ReN-m) and FAD ReN cells (ReN-GA, ReN-mGAP, HReN-mGAP and ReN-mAP). Complementary DNA samples prepared from undifferentiated control ReN-G (1st lane) and human adult brains (9th lane) were used as controls. **e**, **f**, Electrophysiological properties of differentiated control ReN-G cells. The currents were elicited by 10 mV voltage steps from −100 to +60 mV in external solution (**e**) without (left panel in **f**) or with 500 nM tetrodotoxin (TTX, right panel in **f**). TTX treatment specifically blocked voltage-gated sodium currents. ReN-G cells were differentiated for 29 days by the previously described 'preD' method[12]. **g**, Sodium currents are shown as subtracted currents. **h**, Premature ReN-G cells (<16 days) mostly showed voltage-gated potassium currents without TTX-sensitive sodium currents. **i**, Western blot of amyloid-β (Aβ) levels in the conditioned media collected from 6-week differentiated control (ReN-m) and FAD ReN (ReN-mAP and HReN-mGAP) cells. **j**, A table summarizing APOE genotypes of control (ReN-m) and FAD ReN (ReN-mAP) cells used in this study. Two APOE SNP markers, rs429358 (minor allele = C) and rs7412 (minor allele = T), were used to determine APOE ε2/3/4 genotypes.
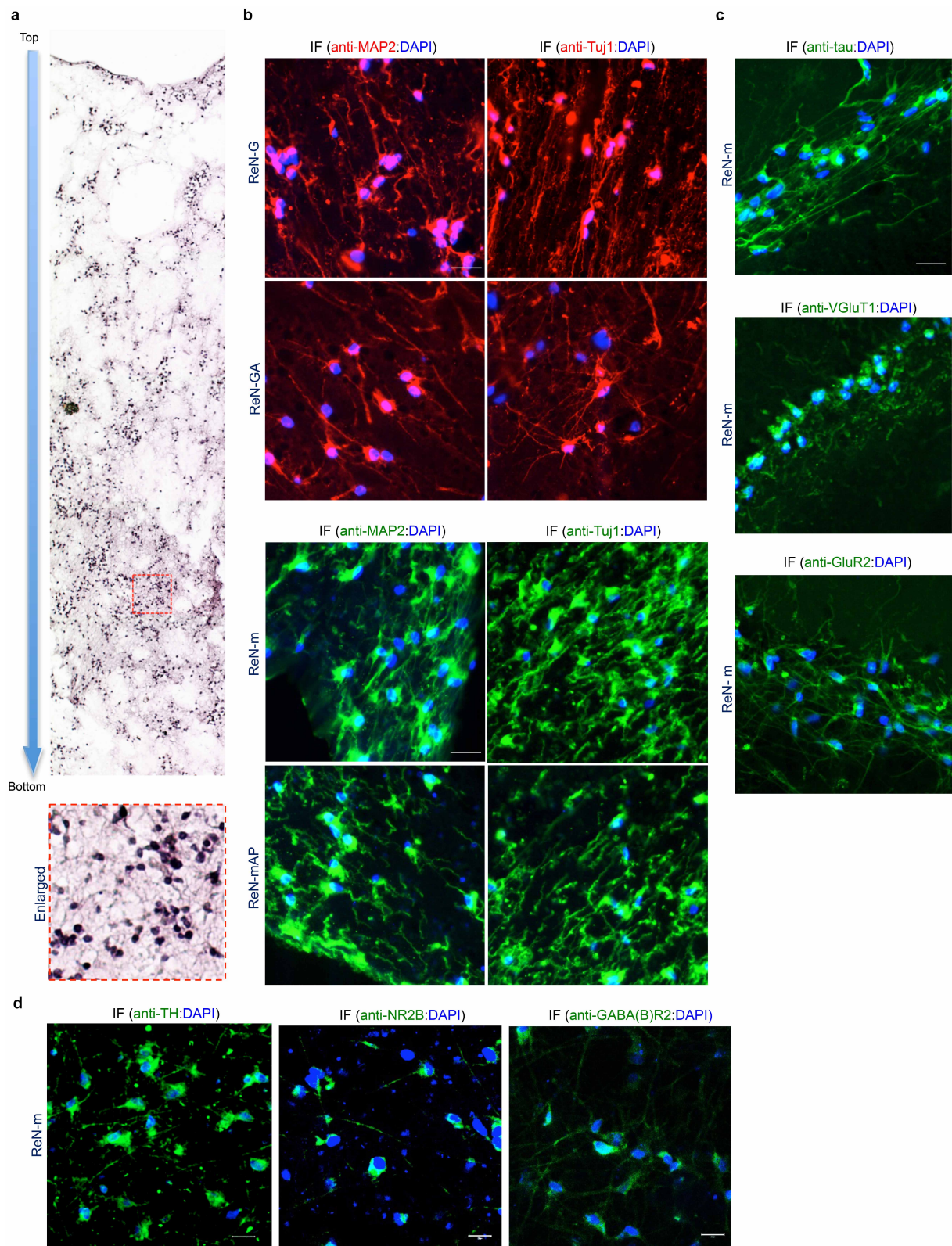
Extended Data Figure 3 | Characterization of differentiated ReN cells in 3D cultures. a, Haematoxylin staining of a representative paraffin section (10 μm) from 9-week differentiated ReN-m cells in thick-layer 3D Matrigel. The sections were vertically cut to show the top and bottom of the 3D cultures. The pictures (10) were serially taken from top to bottom and digitally combined together. Bottom panel represents a digitally magnified image of the respective outlined region for letter visualization; scale bar, 50 μm. **b**, The paraffin sections from control (ReN-G and ReN-m) and FAD ReN (ReN-GA and ReN-mAP (enriched)) were immunofluorescence stained with antibodies against the neuronal markers Tuj1 and MAP2. Blue, DAPI; scale bar, 25 μm. **c**, Immunofluorescence of thick-layer 3D-differentiated ReN-m cells stained with antibodies against additional neuronal markers tau, VGluT1 or GluR2 (glutamate receptor, ionotropic, AMPA 2); scale bar, 25 μm. **d**, Immunofluorescence of 3D-differentiated ReN-m cells (7 weeks) stained with antibodies against mature neuronal markers TH (tyrosine hydroxylase), NR2B (NMDA receptor 2B) or GABA(B)R2 (GABA-B-receptor 2); blue, DAPI; scale bar, 20 μm.

Extended Data Figure 4 | Reconstitution of amyloid-β aggregates in 3D-cultured FAD ReN cells. a, IHC of amyloid-β deposits in control (ReN-G) and FAD ReN (HReN-mGAP) cells differentiated in 3D Matrigel. The control and FAD ReN cells were 3D-differentiated for 6 weeks and then treated with 1 μM BACE1 inhibitor IV (β-secretase inhibitor), 500 nM DAPT (γ-secretase inhibitor), 500 nM SGSM41 (γ-secretase modulator) or DMSO for an additional 3 weeks. The cultures were then fixed and immunostained with HRP-conjugated BA27 anti-Aβ$_{40}$ antibodies (brown, DAB (BA27); blue, haematoxylin; scale bars, 25 μm; arrowhead, large amyloid-β deposits).

b, Enlarged images of amyloid-β deposits in control (ReN-G) and FAD ReN (ReN-mGAP, HReN-mGAP) cell pictures shown in Fig. 2d and Extended Data Fig. 4a. Scale bar, 25 μm. **c**, IHC of amyloid-β deposits in control (ReN-G, left panels) and FAD ReN (ReN-mGAP, middle panels; HReN-mGAP, right panels) cells differentiated in 3D thin-layer Matrigels for 9 weeks. The fixed thin-layer 3D cultures were immunostained with HRP-conjugated BA27 anti-Aβ$_{40}$ antibodies (brown, DAB (BA27); scale bar, 25 mm; arrows, large amyloid-β deposits). **d**, Amylo-Glo staining of ReN-G 3D cultures. Green, GFP; blue, Amylo-Glo; ×10 magnification.
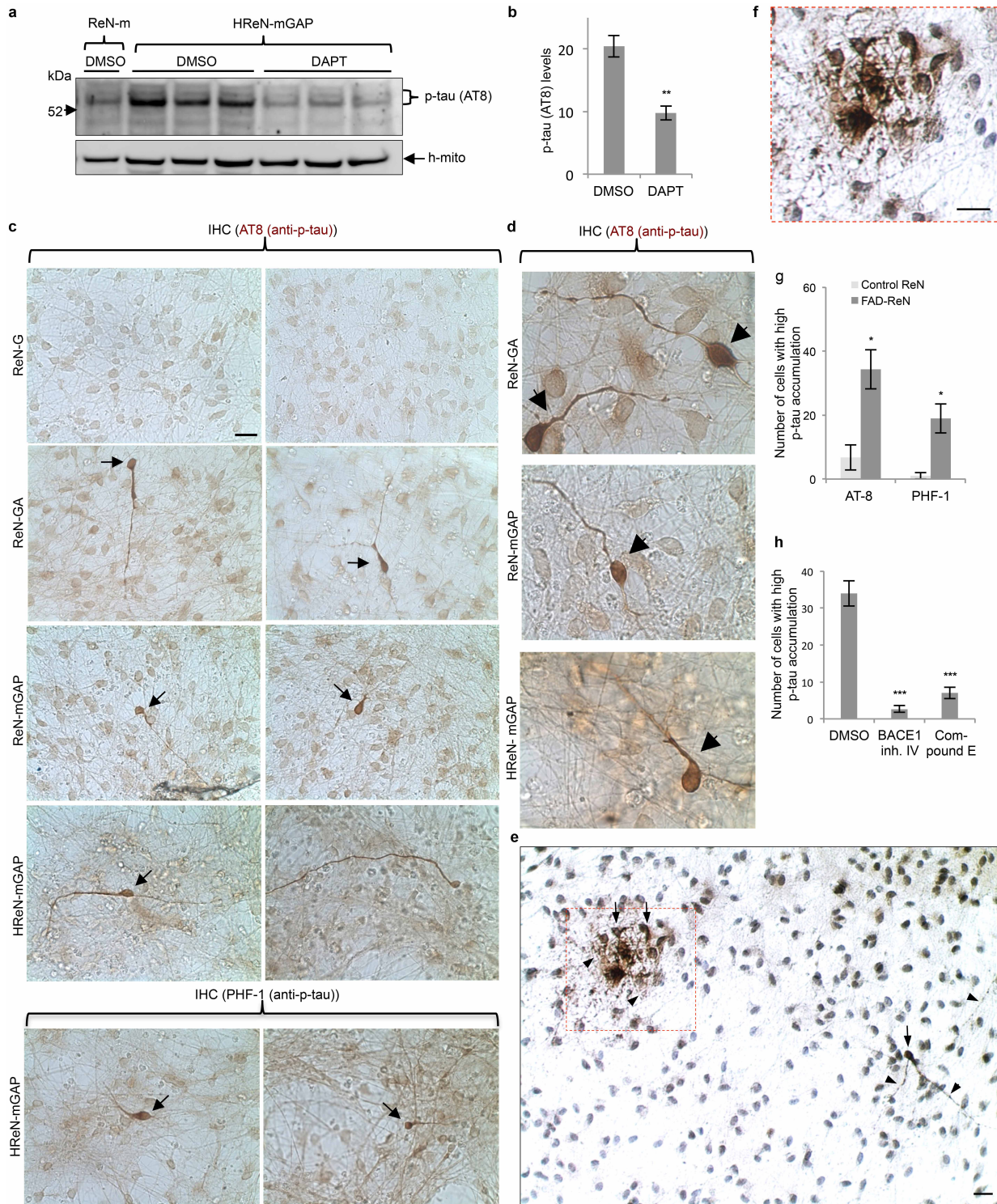
Extended Data Figure 5 | Accumulation of p-tau in FAD ReN cells.
a, Elevated p-tau levels were significantly decreased by 1 μM DAPT (γ-secretase inhibitor) treatment in 6-week differentiated HReN-mGAP cells. The antibody against human specific mitochondrial marker (h-mito) was used to show an equal loading of the samples. **b**, Quantification of p-tau levels in control (DMSO)- and DAPT-treated HReN-mGAP cells (**$P < 0.01$; t-test; $n = 3$ per each sample). y axis values represent relative signal intensities (% adjusted volumes) of each p-tau band. **c**, p-tau IHC showed p-tau-positive cells in 3D-differentiated FAD ReN cells. Two p-tau antibodies, AT8 (pSer 199/Ser 202/Thr 205) and PHF1 (pSer 396/Ser 404), against different phosphorylation sites were used. Brown, p-tau; scale bar, 25 μm; arrows indicate cells with high levels of p-tau. **d**, High magnification (×100) images of p-tau-positive neurons (brown, AT8 p-tau). IHC of AT8 p-tau staining showed neurons with high levels of p-tau accumulation in soma and neurite-like structures (arrowheads). **e**, IHC of p-tau (AT8) staining showed the cells with p-tau accumulations in soma and neurite-like structures (arrow and arrowhead, respectively); scale bar, 25 μm. **f**, A digitally enlarged image of a dotted box in **e**. Brown, p-tau (AT8); blue, haematoxylin; scale bar, 25 μm. **g**, Total number of cells with high levels of p-tau in a single well of a 96-well plate was counted in control (ReN-G and ReN-m) and FAD ReN (ReN-GA, ReN-mGAP and HReN-mGAP) cells (*$P < 0.05$; t-test; $n = 5$ for control ReN cells and $n = 12$ for FAD ReN cells). **h**, BACE1 inhibitor IV (1 μM) or compound E (3.7 nM) treatments markedly decreased the number of cells with high p-tau accumulation in ReN-mAP cell populations (***$P < 0.001$; ANOVA followed by a post hoc Dunnett's test; $n = 3$ for control ReN-m and ReN-mAP cells).
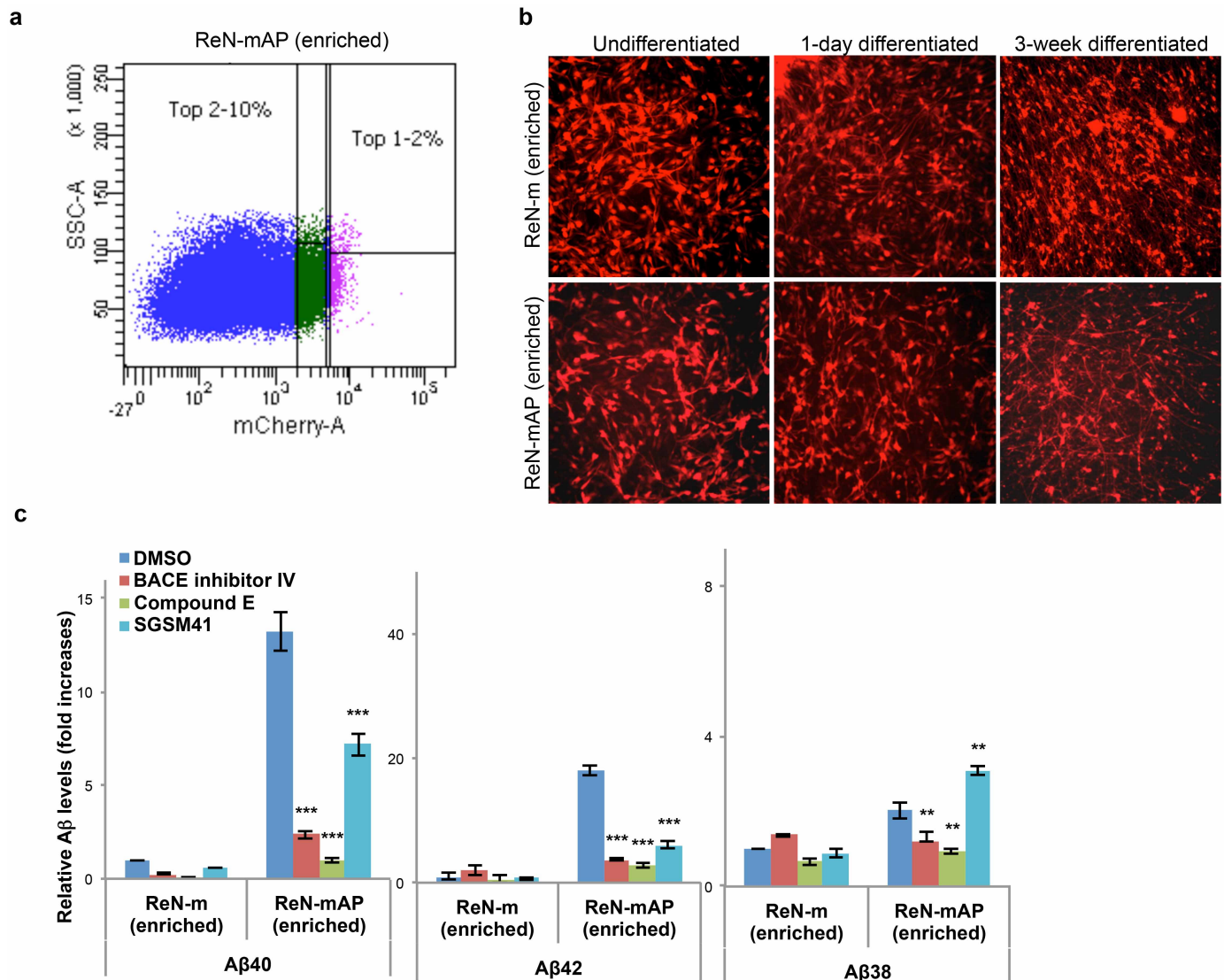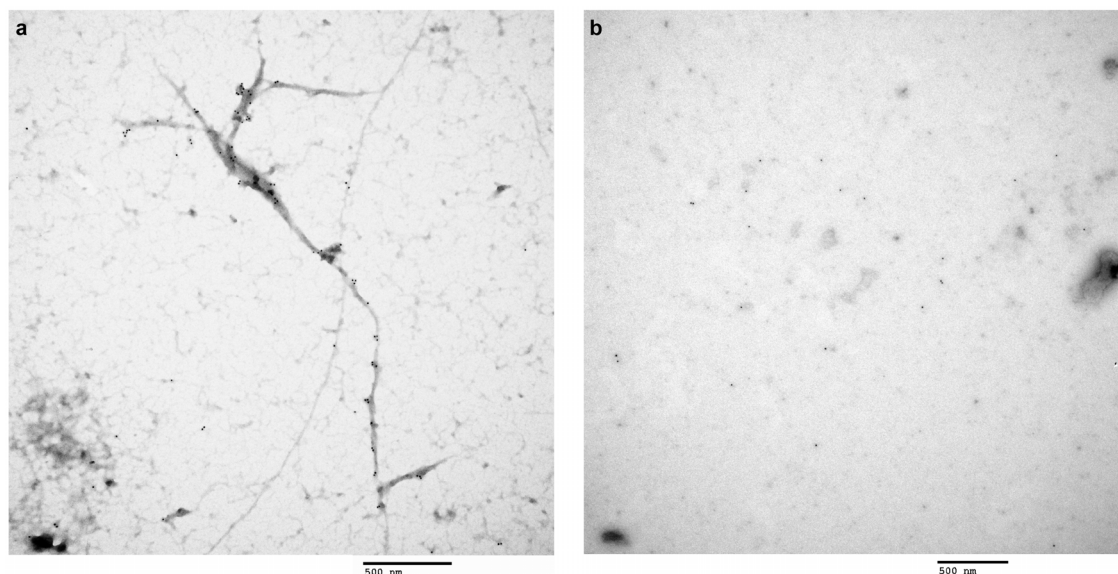
Extended Data Figure 6 | FACS enrichment of ReN-mAP and ReN-m cells for higher expressions of APP and PS1. **a**, FACS sorting of ReN-mAP cells with top 1–2% mCherry signal. mCherry-A, area intensity of mCherry signal. **b**, Representative images of the mCherry-labelled (red), enriched control ReN-m and ReN-mAP cells before or after the differentiation under growth-factor free conditions ($\times$200 magnification); 1- and 3-week differentiated cells show increased neurite outgrowth. **c**, The enriched ReN-mAP cells secreted high levels of $A\beta_{40}$ and $A\beta_{42}$ after 9-week 3D differentiation.

The secreted $A\beta_{38/40/42}$ levels were measured by a multi-array Meso Scale electrochemiluminescence (Meso Scale SQ 120 system). Relative levels of amyloid-β (fold increases) were calculated by setting amyloid-β levels of the control ReN-m as 1. Amyloid-β levels were changed after treating 1 μM BACE1 inhibitor IV, 3.7 nM compound E or 500 nM SGSM41 (**$P < 0.01$; ***$P < 0.001$; ANOVA followed by a post hoc Dunnett's test; $n = 3$ for the enriched ReN-m and ReN-mAP cells).

Extended Data Figure 7 | Increased p-tau levels in FAD ReN cells.
a, Immunofluorescence of AT8 p-tau and Tuj1 in the enriched ReN-mAP and control ReN-m cells after 9 weeks of 3D differentiation. BACE1 inhibitor IV treatment for 3 weeks dramatically reduced AT8 p-tau staining (green, AT8 p-tau; red (pseudo-coloured), Tuj1; scale bar, 25 μm). **b**, Western blot of total

and p-tau levels in control (enriched ReN-m) and FAD ReN (enriched ReN-mAP) cells. The cells were 3D differentiated for 9 weeks. Three weeks of BACE1 inhibitor treatments significantly decreased p-tau levels without changing total tau levels. HSP70 heat shock protein levels are shown to demonstrate equal loading of each sample.

Extended Data Figure 8 | Immunoelectron microscopy analysis of sarkosyl-insoluble fraction from FAD and control ReN cells. a, Sarkosyl-insoluble fractions prepared from 3D-differentiated ReN-mAP (enriched, 7-week differentiated) were placed on carbon grids, labelled with tau_{46} and anti-mouse 10 nm gold antibodies and imaged using a JEOL JEM 1011 transmission electron microscope (scale bar, 500 nm). **b**, Sarkosyl-insoluble fractions from 3D-differentiated control ReN-G cells (7-week differentiated). No immunogold-labelled filamentous structures were detected in these samples (scale bar, 500 nm).
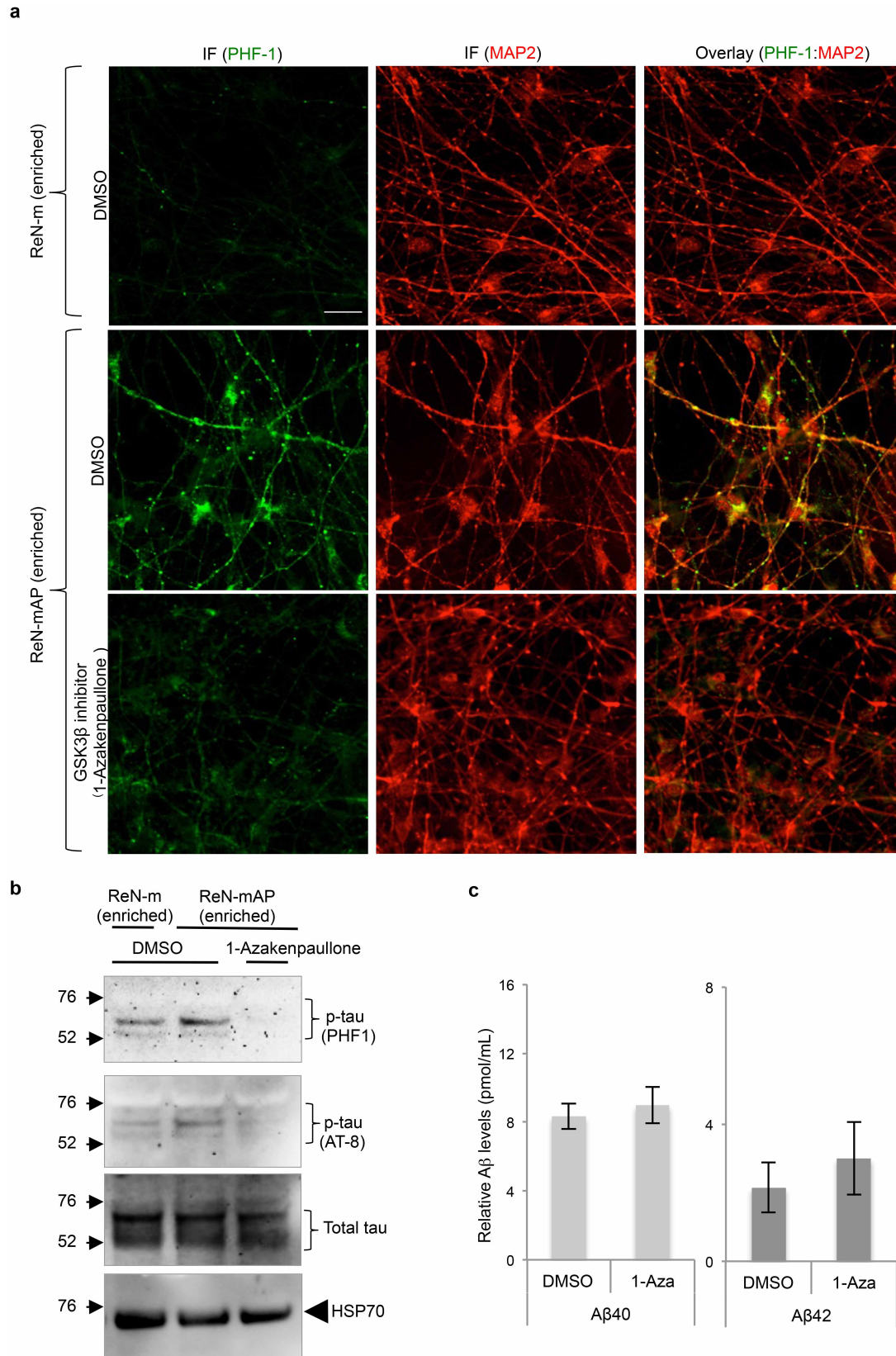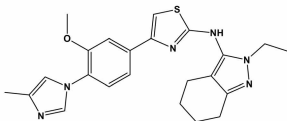
Extended Data Figure 9 | Treatment with 1-azakenpaullone, a GSK3β inhibitor, decreased amyloid-β-induced tau phosphorylation without changing total amyloid-β levels. a, Immunofluorescence of p-tau and MAP2 in the enriched ReN-mAP and control ReN-m cells with or without treatment with 1-azakenpaullone, a GSK3β inhibitor. The differentiated cells were treated with 2.5 μM 1-azakenpaullone or DMSO for the last 5 days of the 3D differentiation (green, p-tau (PHF1); red (pseudo-coloured), MAP2;

scale bar, 25 μm). **b**, Western blot of total and p-tau levels in control (enriched ReN-m) and FAD ReN (enriched ReN-mAP) cells. The cells were 3D differentiated for 4 weeks followed by additional 5-day treatments of DMSO or 2.5 μM 1-azakenpaullone. **c**, Analysis of $A\beta_{40}$ and $A\beta_{42}$ levels in the enriched ReN-mAP cells treated with either DMSO or 2.5 μM 1-azakenpaullone (1-Aza) under the same conditions.

Extended Data Table 1 | The structure and the properties of SGSM41, a novel soluble γ-secretase modulator

Compound	Structure	IC$_{50}$ for the inhibition of Aβ42	IC$_{50}$ for the inhibition of Aβ40	ClogP	Kinetic solubility (μM) in PBS pH 7.4	EC$_{50}$ for the potentiation of Aβ38	Notch	APP	Microsomal Stability % Remaining (human); 30 min	Microsomal Stability % Remaining (rat); 30 min	Microsomal Stability % Remaining (mouse); 30 min
41		115nM	1229nM	4.91	4.6	389nM	NO	NO	28	56	67

SGSM41 has the typical characteristics of this series of SGSM molecules that potently inhibit the production of toxic Aβ$_{42}$, and to a lesser degree Aβ$_{40}$, while concomitantly potentiating the generation of shorter amyloid-β peptide species such as Aβ$_{38}$ and Aβ$_{37}$.